



AD-A199 287

Final Report  
for the period  
July 1987 to  
January 1988

## Distributed Magnetic Actuators for Fine Shape Control

June 1988

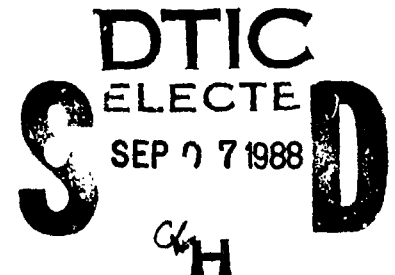
Authors:  
G. Anastas  
D. Eisenhaure  
R. Hockney  
B. Johnson  
K. Misovec

SatCon Technology Corporation  
71 Rogers Street  
Cambridge, MA 02142

R01-88  
F04611-87-0047

### Approved for Public Release

Distribution is unlimited. The AFAL Technical Services Office has reviewed this report, and it is releasable to the National Technical Information Service, where it will be available to the general public, including foreign nationals.



prepared for the:

**Air Force  
Astronautics  
Laboratory**

Air Force Space Technology Center  
Space Division, Air Force Systems Command  
Edwards Air Force Base,  
California 93523-5000

88 9 6 19 9

## NOTICE


When U.S. Government drawings, specifications, or other data are used for any purpose other than a definitely related Government procurement operation, the fact that the Government may have formulated, furnished, or in any way supplied the said drawings, specifications, or other data, is not to be regarded by implication or otherwise, or in any way licensing the holder or any other person or corporation, or conveying any rights or permission to manufacture, use, or sell any patented invention that may be related thereto.

## FOREWORD

This final report was submitted by SatCon Technology Corporation, Cambridge, MA on completion of SBIR contract F04611-87-C-0047 with the Air Force Astronautics Laboratory (AFAL), Edwards Air Force Base, CA. AFAL Project Manager was Capt Eric Dale.

This report has been reviewed and is approved for release and distribution in accordance with the distribution statement on the cover and on the DD Form 1473.

  
ERIC M. DALE, CAPT, USAF  
Project Manager

  
L. KEVIN SLINAK  
Chief, Interdisciplinary Space  
Technology Branch

FOR THE COMMANDER

  
DAVID J. OLKOWSKI, Major, USAF  
Deputy Director  
Aerospace Vehicle Systems Division

| REPORT DOCUMENTATION PAGE  |       |  |  | Form Approved<br>OMB No. 0704-0188                   |                                   |
|--|-------|--|--|--|-----------------------------------|
| 1a. REPORT SECURITY CLASSIFICATION<br><b>Unclassified</b>  |       |  | 1b. RESTRICTIVE MARKINGS<br><b>None</b>  |  |                                   |
| 2a. SECURITY CLASSIFICATION AUTHORITY  |       |  | 3. DISTRIBUTION/AVAILABILITY OF REPORT<br><b>Approved for public release; distribution is unlimited.</b>   |  |                                   |
| 2b. DECLASSIFICATION/DOWNGRADING SCHEDULE  |       |  |  |  |                                   |
| 4. PERFORMING ORGANIZATION REPORT NUMBER(S)<br><b>R01-88</b>   |       |  | 5. MONITORING ORGANIZATION REPORT NUMBER(S)<br><b>AFAL-TR-88-026</b>   |  |                                   |
| 6a. NAME OF PERFORMING ORGANIZATION<br><b>SatCon Technology Corporation</b>  |       | 6b. OFFICE SYMBOL<br>(if applicable)<br><b>1JB94</b> | 7a. NAME OF MONITORING ORGANIZATION<br><b>Air Force Astronautics Laboratory</b>  |  |                                   |
| 6c. ADDRESS (City, State, and ZIP Code)<br><b>71 Rogers Street<br/>Cambridge, MA 02142</b>   |       |  | 7b. ADDRESS (City, State, and ZIP Code)<br><b>AFAL/VSSS<br/>Edwards AFB, CA 93523-5000</b>   |  |                                   |
| 8a. NAME OF FUNDING/SPONSORING ORGANIZATION  |       | 8b. OFFICE SYMBOL<br>(if applicable)                 | 9. PROCUREMENT INSTRUMENT IDENTIFICATION NUMBER<br><b>F04611-87-C-0047</b>   |  |                                   |
| 8c. ADDRESS (City, State, and ZIP Code)  |       |  | 10. SOURCE OF FUNDING NUMBERS  |  |                                   |
|  |       |  | PROGRAM ELEMENT NO.<br><b>65502F</b>   | PROJECT NO.<br><b>2864</b>                           | TASK NO.<br><b>00</b>             |
| 11. TITLE (Include Security Classification)<br><b>Distributed Magnetic Actuators for Fine Shape Control (U)</b>  |       |  |  |  |                                   |
| 12. PERSONAL AUTHOR(S)<br><b>George Anastas, David Eisenhaure, Richard Hockney, Bruce Johnson, Kathleen Misovec</b>  |       |  |  |  |                                   |
| 13a. TYPE OF REPORT<br><b>Final</b>  |       | 13b. TIME COVERED<br>FROM <b>87/7</b> TO <b>88/1</b> |  | 14. DATE OF REPORT (Year, Month, Day)<br><b>88/6</b> |                                   |
| 15. PAGE COUNT<br><b>91</b>  |       |  |  |  |                                   |
| 16. SUPPLEMENTARY NOTATION   |       |  |  |  |                                   |
| 17. COSATI CODES   |       |  | 18. SUBJECT TERMS (Continue on reverse if necessary and identify by block number)<br><b>Distributed Actuators      Large Space Structures<br/>Vibration Control      Shape Control<br/>Magnetic Magnetostrictive</b> |  |                                   |
| FIELD  | GROUP | SUB-GROUP  |  |  |                                   |
| 22   | 02    |  |  |  |                                   |
| 20   | 03    |  |  |  |                                   |
| 19. ABSTRACT (Continue on reverse if necessary and identify by block number)<br><br>New spacecraft designs feature large structures characterized by low natural frequencies and stringent pointing and vibration requirements. These large space structures pose unique and difficult control problems. These problems include system bandwidths greater than structural natural frequencies; lack of accurate information about the dynamic characteristic of the structure being controlled; complicated high-order dynamics, including non-linear behavior; and stringent requirements for distributed shape control. An important part of the solution to these control problems is the development of actuators capable of applying force or torque to the structures. Conventionally these actuators have been reaction mass actuators or distributed piezoelectric materials.<br>→ The objective of this research program was to investigate other innovative actuator designs for use in flexible spacecraft structure control. In particular, actuators based (continued on reverse) |       |  |  |  |                                   |
| 20. DISTRIBUTION/AVAILABILITY OF ABSTRACT<br><input type="checkbox"/> UNCLASSIFIED/UNLIMITED <input checked="" type="checkbox"/> SAME AS RPT. <input type="checkbox"/> DTIC USERS  |       |  | 21. ABSTRACT SECURITY CLASSIFICATION<br><b>Unclassified</b>  |  |                                   |
| 22a. NAME OF RESPONSIBLE INDIVIDUAL<br><b>Eric M. Dale, Capt., USAF</b>  |       |  | 22b. TELEPHONE (Include Area Code)<br><b>(805) 275-5483</b>  |  | 22c. OFFICE SYMBOL<br><b>VS3S</b> |

19. ABSTRACT (cont.)

on the direct use of electromagnetic forces were developed. Originally the focus of this research program was to develop actuator concepts based on the Lorentz force interactions of current-carrying wires. These concepts range from discrete, distributed coils interacting with Earth's magnetic field to distributed winding patterns embedded in the space structure. In addition to the original focus, this Phase II program expanded its focus to investigate the applicability of magnetostrictive materials to shape control actuators. This expanded focus was the result of the recent development of the high-performance magnetostrictive material Terfenol-D. This new material offers a factor of 10 improvement in both strain capability and energy density compared to piezoelectric materials.

The major expected advantages of these advanced actuators include high bandwidth, compatibility with composite structures, and low mass. A variety of concepts were developed, some of which have application to different types of flexible structures including those with combined attitude and flexible structure control. One concept was identified as most feasible for more general types of flexible structure applications such as space robotic arms, deployable truss structures, or flexible antennas. This concept is a local coil interaction scheme that has coils placed very close to each other in structural sections. (jkd)

The key technology development required for these actuators is integration of the actuators into a structural component and the controllers associated with the actuators. The proposed Phase II research will analytically compare the local interaction concept and the magnetostrictive actuator concept. Both concepts will then be designed in detail, constructed, tested, and compared as laboratory prototype actuators embedded in a structural section.



|                  |                                     |
|------------------|-------------------------------------|
| Accession For    |                                     |
| NTIS GRA&I       | <input checked="" type="checkbox"/> |
| DTIC TAB         | <input type="checkbox"/>            |
| Unannounced      | <input type="checkbox"/>            |
| Justification    |                                     |
| By               |                                     |
| Distribution/    |                                     |
| Availability Co. |                                     |
| Dist             | Avail and/or Special                |
| A-1              |                                     |

## TABLE OF CONTENTS

| <u>Section</u>  | <u>Page</u> |
|---|-------------|
| INTRODUCTION . . . . .  | 1           |
| MODEL DEVELOPMENT. . . . .  | 4           |
| - Overview of the Model Requirements . . . . .  | 4           |
| - The Finite Element Method for a<br>General Structure. . . . .                                       | 5           |
| - Finite Element Equations for a<br>2-degree-of-freedom Cantilever Beam. . . . .                      | 11          |
| - Dynamic Characteristics of the Beam Model. . . . .  | 16          |
| ACTUATOR DESIGN. . . . .  | 18          |
| - Magnetic Analysis Methods. . . . .  | 18          |
| - Magnetic Forces. . . . .  | 18          |
| - Far-Field Approximation. . . . .  | 20          |
| - Example "Standard" Dipole. . . . .  | 22          |
| - Maxwell's Mutual Inductance Formula<br>for Circular Filaments . . . . .                             | 24          |
| ACTUATOR APPROACHES. . . . .  | 26          |
| - Interaction of Distributed Coils with<br>Earth's Magnetic Field . . . . .                           | 27          |
| - Interaction of Distributed Coils with a<br>Large Flux Source. . . . .                               | 30          |
| - Interaction of Distributed Coils . . . . .  | 33          |
| - Local Interaction of Magnetic Coils<br>on a Truss Section . . . . .                                 | 44          |
| - Use of Magnetostrictive Material . . . . .  | 48          |
| - Magnetostriction . . . . .  | 48          |
| - Summary of Actuator Design Section . . . . .  | 56          |
| COMPARISON OF ACTUATOR APPROACHES. . . . .  | 56          |
| - Force Comparison . . . . .  | 57          |
| - Control Effectiveness and Optimum Actuator<br>Location Derivation of Control Effectiveness. . . . . | 59          |
| - Comparison of Control Effectiveness for<br>Distributed and Local Cases. . . . .                     | 62          |
| - Summary of Actuator Comparison Section . . . . .  | 74          |
| CONTROLLER DESIGN. . . . .  | 75          |
| CONCLUSIONS. . . . .  | 76          |

# LIST OF ILLUSTRATIONS

| Figure |  | Page           |
|--------|--|----------------|
| 1      | Artist's Conception of MAST Structure . . . . .  | 6              |
| 2      | General Three-Dimensional Body. . . . .  | 7              |
| 3      | Cantilever Beam, Discretized Model, and<br>Beam Element. . . . .   | 12             |
| 4      | Element Stiffness Matrix and Element Mass Matrix. . . . .  | 15             |
| 5      | Mode Shapes . . . . .  | 17             |
| 6      | Two Current Loops . . . . .  | 19             |
| 7      | Spherical Coordinate System . . . . .  | 21             |
| 8      | Two Interacting Dipoles . . . . .  | 22             |
| 9      | "Standard" Size Coil. . . . .  | 23             |
| 10     | Configuration for Example Calculations of<br>Interaction Force and Torque on Two<br>Standard Size Coils . . . . .  | 24             |
| 11     | Two Coaxial Equal-radius Circular Filaments . . . . .  | 25             |
| 12     | Near Field Filament Interaction Force . . . . .  | 26             |
| 13     | Actuator Approach 1: Interaction of Distributed<br>Coils with Earth's Magnetic Field . . . . .   | 28             |
| 14     | Earth's Magnetic Field vs Altitude. . . . .  | 29             |
| 15     | Actuator Approach 2: Interaction of Distributed<br>Coils with Large Flux Source. . . . .   | 31             |
| 16     | Large Flux Source Solenoid Dimensions . . . . .  | 32             |
| 17     | Actuator Approach 3: Interaction of Distributed<br>Coils . . . . .   | 34             |
| 18     | Configuration of Distributed Coils and Their<br>Associated Dipole Interaction Force/Torque<br>Expressions<br>(a) Configuration 1 . . . . .<br>(b) Configuration 2 . . . . .<br>(c) Configuration 3 . . . . . | 35<br>36<br>37 |
| 19     | Configuration of Distributed Coils which Produces<br>Both Force and Torques Suitable for Beam Bending<br>Control . . . . .   | 38             |
| 20     | Force vs Separation Distance for Configuration 1. . . . .  | 39             |
| 21     | Force and Torque Separation Distance for<br>Configuration 2 . . . . .  | 40             |
| 22     | Force vs Separation Distance for Configuration 3. . . . .  | 41             |
| 23     | Force vs Current Density for Configuration 1. . . . .  | 41             |
| 24     | Force and Torque vs Current Density for<br>Configuration 3 . . . . .   | 42             |
| 25     | Force vs Current Density for Configuration 3. . . . .  | 43             |
| 26     | Actuator Approach 4: Local Coil Interaction. . . . .   | 44             |
| 27     | Extreme Models of Beam-Truss Interaction for<br>Local Actuator Approach . . . . .  | 46             |
| 28     | Magnetostriction of Terfenol-D vs Applied<br>Magnetic Field. . . . .   | 50             |
| 29     | Simple Magnetostrictive Actuator. . . . .  | 52             |
| 30     | Example Stress Waveform in Terfenol-D . . . . .  | 53             |

# List of Illustrations (Continued)

| <u>Figure</u> |  | <u>Page</u> |
|---------------|--|-------------|
| 31            | Example Applied Magnetic Field Waveform in Terfenol-D. . . . .   | 53          |
| 32            | Stress vs Strain in the Terfenol-D for the Example Waveforms . . . . .   | 54          |
| 33            | Mass Comparison of Local vs Distributed Actuator Concepts . . . . .  | 59          |
| 34            | Power Comparison of Local vs Distributed Actuator Concepts . . . . .   | 60          |
| 35            | Modelling Assumptions Appropriate for Use in Finite Element Beam Model for Local Interaction Actuator Schemes. . . . . | 63          |
| 36            | Definition of Mean Location, $\alpha$ , and Coil Separation, $\beta$ , for Sinusoidal Mode Shape. . . . .              | 66          |
| 37            | Control Effectiveness vs Coil Separation. . . . .  | 68          |
| 38            | Control Effectiveness vs Coil Separation. . . . .  | 69          |
| 39            | Time Simulations for Controlled Beam Using Two Truss Tension-Tension Local Interaction Scheme. . . . .                 | 77          |
| 40            | Time Simulations for Controlled Beam Using Two Truss Tension-Compression Local Interaction Scheme. . . . .             | 78          |

## LIST OF TABLES

| <u>Table</u> |  | <u>Page</u> |
|--------------|--|-------------|
| 1            | Physical Parameters of Beam Model . . . . .                                    | 16          |
| 2            | Lowest Four Natural Frequencies of<br>35 Element Model. . . . .                | 17          |
| 3            | Terfenol-D Properties . . . . .  | 55          |
| 4            | Effectiveness Expressions for Local and<br>Distributed Actuator Types. . . . . | 67          |
| 5            | Effectiveness Calculations. . . . .  | 71          |
| 6            | Effectiveness Calculations. . . . .  | 73          |
| 7            | Effectiveness Calculations. . . . .  | 74          |

## INTRODUCTION

New spacecraft designs feature large structures characterized by low natural frequencies and stringent pointing and vibration requirements. These large space structures pose unique and difficult control problems. These problems include system bandwidths greater than structural natural frequencies; lack of accurate information about the dynamic characteristic of the structure being controlled; complicated high-order dynamics, including non-linear behavior; and stringent requirements for distributed shape control<sup>1</sup>. An important part of the solution to these control problems is the development of actuators capable of applying force or torque to the structures. Conventionally these actuators have been reaction mass actuators or distributed piezoelectric materials.

The motivation of this research is to investigate other innovative actuator designs. In particular, the direct use of electromagnetic forces is seen as a promising approach. Originally the focus of this research program was to develop actuator concepts based on the Lorentz force interactions of current carrying wires. These concepts range from discrete, distributed coils interacting with Earth's magnetic field to distributed winding patterns embedded in the space structure. These actuators are expected to have a number of advantages including high bandwidth, compatibility with composite structures, and low mass. In addition to the original focus,

this Phase I program expanded its focus to investigate the applicability of magnetostrictive materials to shape and vibration control actuators. This expanded focus was the result of the recent development of high performance magnetostrictive material Terfenol-D. This new material offers a factor of 10 improvement in both strain capability and energy density compared to piezoelectric materials.

The research was divided into six tasks. First a flexible structure model appropriate for control and actuator assessment was developed. The next two tasks investigated actuator placement issues and developed design definitions for the advanced actuator. The fourth task developed controller algorithms. The fifth task evaluated the performance of the controlled structure using the magnetic coil actuators. The sixth task investigated the effect of these actuators on system issues such as interference with the Earth's magnetic field.

This report is organized as follows. The first major section explains the model development. A flexible beam model of the MAST deployable truss space structure was used for this study. In the next major section, which is the main emphasis of this research, issues pertaining to actuator design are discussed and an initial analysis is performed on each design method. The magnetic analysis methods needed are reviewed briefly. Five actuator designs are identified. The first is the interaction of magnetic coils with the Earth's magnetic field. The second is the interaction of the magnetic coils with a large flux source on

another part of the spacecraft. These two types of actuators are shown to be undesirable for the NAST application yet could have advantages for control of other types of flexible structures. The third is the interaction of distributed magnetic coils on the flexible beam structure. The fourth is the local interaction of magnetic coils placed very close together. The final approach is the use of a new magnetostrictive material called Terfenol-D to control the beam through strain. Magnetostriction is the property of some materials to strain under the presence of a magnetic field. The design and analysis of these approaches involved investigations into system issues and actuator placement issues.

In the next major section, two of the more promising methods the distributed coil interaction and the local coil interaction are compared in more detail. Specifically, the control effectiveness of the actuators, which is based on excitation mode and actuator location, is derived and compared. The local interaction method is shown to be more effective than the distributed on both a per mass and a per power basis. The use of Terfenol-D is also a very promising method, as is shown; however, more comparison analysis needs to be done. It is proposed that comparisons of the local interaction and the magnetostrictive actuator approaches be performed as an initial task for Phase II research. The purpose of the next major section, Controller Design, is to illustrate how the local interaction actuators may be used in controlling a beam structure and to verify the control

effectiveness concepts that were developed. The final section is the conclusions section.

## MODEL DEVELOPMENT

This section outlines the method that was used to obtain a large flexible structure model which is appropriate to the investigation of distributed magnetic actuators. The model used is a mathematical representation of the MAST deployable space truss structure, which has a lowest natural frequency of 0.2 Hz. This section contains an overview of the model requirements<sup>2</sup>, a derivation of the finite element equations for the structure, and finally a presentation of the structure's dynamic characteristics.

### Overview of the Model Requirements

The main purpose of this study is to assess the advantages that can be gained by using distributed magnetic actuators to achieve structural shape and vibration control. In order to meet this goal, a flexible structure model is needed so that the closed-loop performance of the controlled structure with the actuators can be evaluated. This section outlines some of the desired features of the flexible structure model.

The ideal model is complex enough to reflect flexible structure dynamical features, such as low natural frequencies and lightly damped structural modes. On the other hand, the model must be simple enough to be analytically tractable and produce

useful general insights into system behavior. In order to be compatible with the control software tools which will be used, the model must be reducible to a finite state format.

To satisfy these model requirements, a two degree-of-freedom finite element cantilevered beam model subject to transverse shear forces and bending moments was chosen for this study. A beam was chosen because it can be an appropriate simplified model for many different types of flexible structures; for example, a beam could be a simple model of a robotic arm or a deployable truss structure. The actual parameters for this beam model are compatible with the MAST structure. This structure is a 60 m long deployable truss structure which was designed to be used on space shuttle missions<sup>3</sup>. Figure 1 is an artist's conception of MAST<sup>4</sup>. Because the shuttle is much more massive than the structure, a cantilever beam is a good model of the system. Although this NASA program is now cancelled, similar flexible structures are likely for implementation in future space programs. The finite element equations of the beam were manipulated to obtain a finite state representation of the model.

#### **The Finite Element Method for a General Structure**

The finite element method is based on the principle of virtual work which states that equilibrium of a body requires that for any compatible, small virtual displacements (which satisfy the geometric boundary conditions), the total internal virtual work is equal to the total external virtual work.

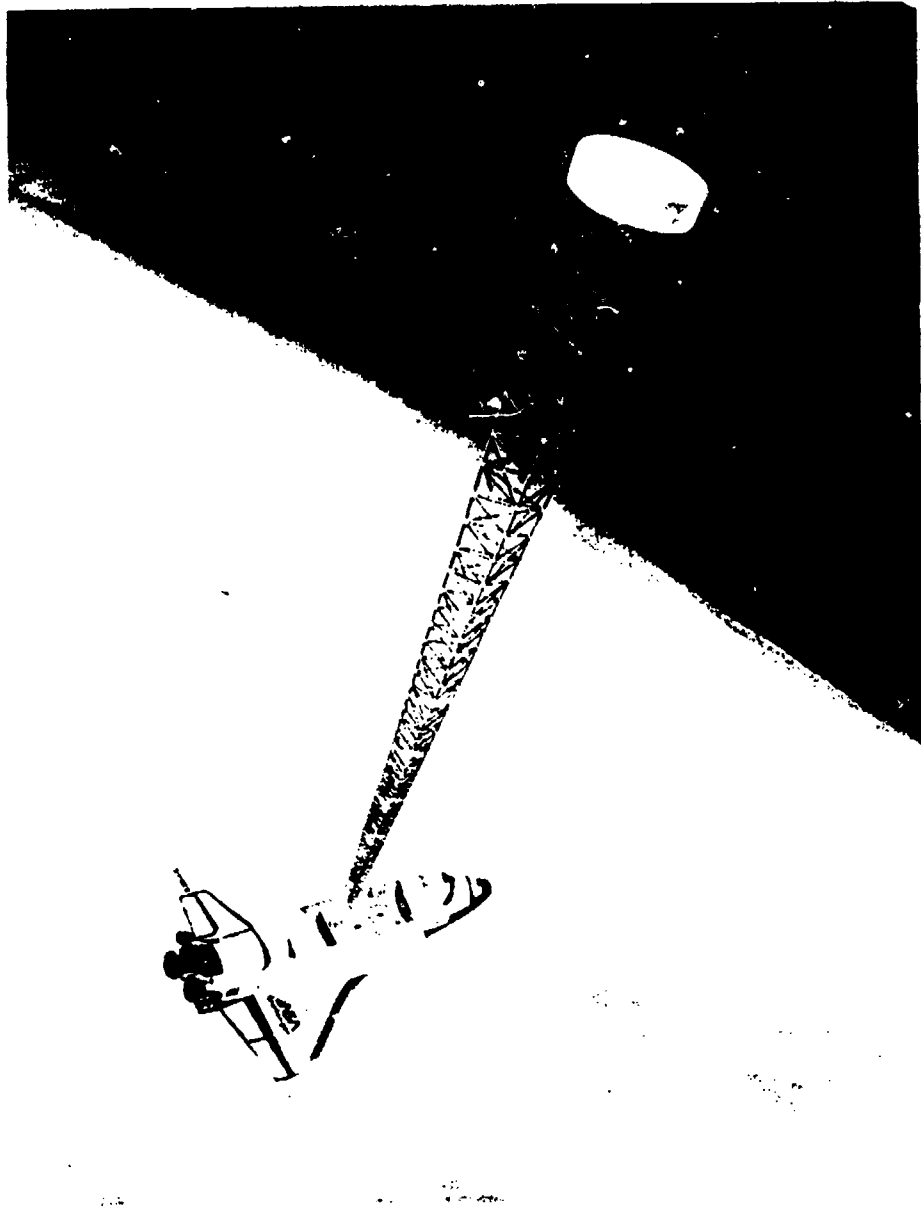


Figure 1 Artist's Conception of MAST Structure<sup>5</sup>

Therefore, for a general three-dimensional body such as shown in Figure 2, the principle can be stated as follows:

$$\int_V \bar{\epsilon}'_r dv = \int_V \bar{U}' f^B dv + \int_S \bar{U}' f^S ds + \sum_i U^i f^i \quad (1)$$

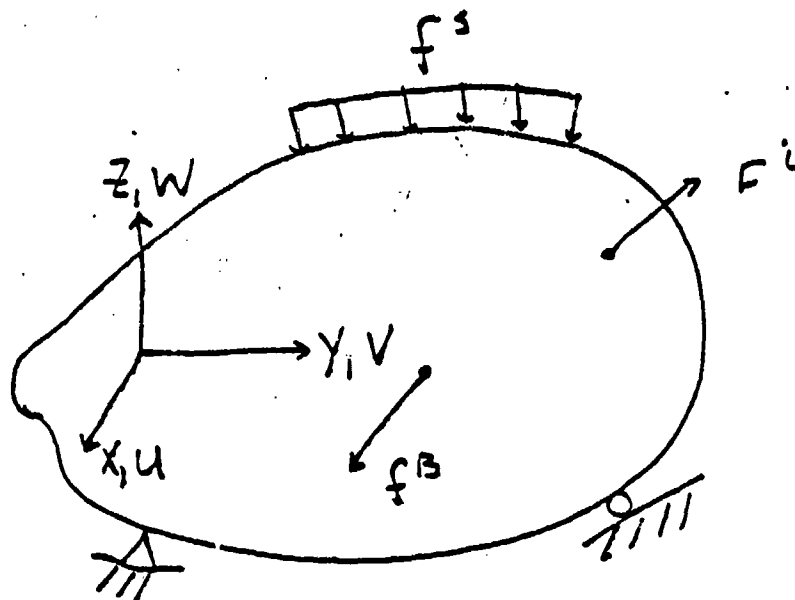


Figure 2 General Three-Dimensional Body

where the overbar denotes virtual quantities, and

$$\bar{f}^B = [ \bar{f}_x^B \bar{f}_y^B \bar{f}_z^B ]' = \text{Externally Applied Body Forces}$$

$$\bar{f}^S = [ \bar{f}_x^S \bar{f}_y^S \bar{f}_z^S ]' = \text{Externally Applied Surface Forces}$$

$$\bar{F}^i = [ \bar{F}_x^i \bar{F}_y^i \bar{F}_z^i ]' = \text{Externally Applied Concentrated Forces}$$

$$\bar{U}' = [ \bar{U} \bar{V} \bar{W} ]' = \text{Body Displacements}$$

$$\bar{\epsilon} = [ \bar{\epsilon}_{xx} \bar{\epsilon}_{yy} \bar{\epsilon}_{zz} \bar{\gamma}_{xy} \bar{\gamma}_{yz} \bar{\gamma}_{zx} ]' = \text{Body Strains}$$

$$\bar{\sigma} = [ \bar{\sigma}_{xx} \bar{\sigma}_{yy} \bar{\sigma}_{zz} \bar{\sigma}_{xy} \bar{\sigma}_{yz} \bar{\sigma}_{zx} ]' = \text{Body Stresses}$$

$$V = \text{Volume}$$

$$S = \text{Surface Area}$$

Although Equation (1) is an expression of equilibrium, it can also satisfy constitutive and compatibility requirements if the problem is formulated properly<sup>6</sup>.

The general procedure of any finite element problem begins with approximating the body as an assemblage of discrete finite elements which are interconnected at nodal points. The next step is to obtain individual element equations which satisfy the

constitutive and compatibility requirements<sup>7</sup>.

Element stresses can be related to element strains by the elasticity matrix (Equation (2)). When this relationship is incorporated into the principle of virtual work, constitutive requirements are satisfied<sup>8</sup>.

$$\sigma^m = C^m \epsilon^m + \sigma^{Im} \quad (2)$$

$C^m$  = Elasticity Matrix for Element

$\sigma^{Im}$  = Element Initial Stress Vector

$\epsilon^m$  = Element Strain Vector

For compatibility requirements, first a displacement interpolation matrix,  $H^m$ , is formulated to relate internal element displacements to displacements at nodal points (Equation (3)). Strain-displacement relations can then be satisfied by appropriate manipulations of the displacement interpolation matrix (Equation (4))<sup>9</sup>.

$$u^m(x,y,z) = H^m(x,y,z) U \quad (3)$$

$u^m$  = Element Displacement Vector

$U$  = Vector of Global Displacements at Nodal Points

$$\epsilon^m(x,y,z) = B^m(x,y,z) U \quad (4)$$

$B^m$  = Strain Displacement Matrix

The last step of the finite element method is to assemble the individual element equations in order to satisfy the principle of virtual work.

$$\sum_m \int_{V^m} \bar{\epsilon}^m, \sigma^m dV^m = \sum_m \int_{V^m} \bar{U}^m, f^B dV^m + \sum \int_{S^m} \bar{U}^m S, f^S dS^m + \sum_i \bar{U}^i, F^i \quad (5)$$

In the above expression, the element contributions to the virtual work are calculated by integrating over the elemental volume,  $v^m$ , or surface area,  $s^m$ , appropriately; and the contributions of all the elements are summed up to obtain the total virtual work. By substituting Equations (2), (3), and (4) into Equation (5), compatibility, constitutive, and equilibrium requirements can be satisfied<sup>10</sup>.

$$\begin{aligned} \bar{U}' \left[ \sum_m \int_{v^m} B^m, C^m B^m dv^m \right] U = & \bar{U}' \left[ \left( \sum_m \int_{v^m} H^m, f^B B^m dv^m \right) \right. \\ & + \left( \sum_m \int_{s^m} H^{Sm}, f^{Sm} ds^m \right) \\ & \left. - \left( \sum_m \int_{v^m} B^m, r^I dv^m \right) + F \right] \end{aligned} \quad (6)$$

Since the principle of virtual work is satisfied for any arbitrary virtual displacements, which do not violate geometric boundary conditions, all of the virtual displacements can be set equal to one. Equation (6) can now be rewritten as:

$$K U = R \quad (7)$$

$$K = \sum_m \int_{v^m} B^m, C^m B^m dv^m = \sum_m K^m$$

$$R = R_B + R_S - R_I + R_C$$

$$R_B = \sum_m \int_{v^m} H^m, f^B B^m dv^m = \sum_m R_B^m$$

$$R_S = \sum_m \int_{S^m} H^{Sm}, f^{Sm} dS^m = \sum_m R_S^m$$

$$R_I = \sum_m \int_{V^m} B^m, r^I dV^m = \sum_m R_I^m$$

$$R_C = F = \sum_m R_C^m$$

D'Alembert's principle can be invoked to incorporate dynamic effects into the model (Equation (8) and Equation (9)).

$$R_B = \sum_m \int_{V^m} H^m, (f^{Bm} - \rho^m H^m \ddot{U}) dV^m \quad (8)$$

$$U = dU^2 / dt^2$$

$$\rho^m = \text{Mass density of element } m$$

$$M = \sum_m \int_{V^m} \rho^m H^m, H^m dV^m = \sum M^m \quad (9)$$

Therefore, the finite element equations for a general body are<sup>11</sup>:

$$M \ddot{U} + K U = R \quad (10)$$

Boundary conditions are imposed by splitting up the problem into known displacements and unknown displacements and then expressing the unknown displacements in terms of the known displacements (Equations (11) and (12)). The resultant set of equations has the same "spring-mass" form as the original set of equations, only the load vector is modified in such a way that boundary conditions are satisfied.

$$\begin{bmatrix} M_{aa} & M_{ab} \\ M_{ba} & M_{bb} \end{bmatrix} \begin{bmatrix} \ddot{U}_a \\ \ddot{U}_b \end{bmatrix} + \begin{bmatrix} K_{aa} & K_{ab} \\ K_{ba} & K_{bb} \end{bmatrix} \begin{bmatrix} U_a \\ U_b \end{bmatrix} = \begin{bmatrix} R_a \\ R_b \end{bmatrix} \quad (11)$$

$U_a$  = Prescribed Displacements

$U_b$  = Unknown Displacements

$$M_{bb} \ddot{U}_b + K_{bb} U_b = R_b - M_{ba} \ddot{U}_a - K_{ba} U_a \quad (12)$$

Once the unknown displacements have been solved for, the unknown loads can be obtained as is shown in Equation (13).

$$R_a = M_{aa} \ddot{U}_a + M_{ab} \ddot{U}_b + K_{aa} U_a + K_{ab} U_b \quad (13)$$

#### Finite Element Equations for a 2-degree-of-freedom Cantilever Beam

The flexible structure model used in this study was a cantilevered beam subject to shear forces and bending moments. A computer program was developed to give the finite element equations for a cantilevered beam with variable length elements,  $l$  (see Figure 3). The beam used has a constant cross-sectional area as shown. The element is described by axial, transverse, and rotational displacements. Axial displacements are later dropped from the final equations because the bending behavior is of more interest than the axial behavior. Allowing the program to have a variable number of variable length elements gives some degree of control over the complexity of analysis.

A 35, 140 state element model was used for natural frequency and mode shape computations. Models with fewer elements were used for controller design.

The finite element equations for the cantilever beam

neglecting damping can be written as follows:

$$M U + K U = R \quad (14)$$

$$K = \sum_{m=1}^{N+1} K^m$$

$$M = \sum_{m=1}^{N+1} M^m$$

$$U = [ u_1 \ w_1 \ \theta_1 \ w_2 \ \theta_2 \ \dots \ u_{N+1} \ w_{N+1} \ \theta_{N+1} ]'$$

= (Nodal Displacement Vector)

$$R = [ F_1 \ M_1 \ F_2 \ M_2 \ \dots \ F_{N+1} \ M_{N+1} ]'$$

= (Concentrated Nodal Force Vector)

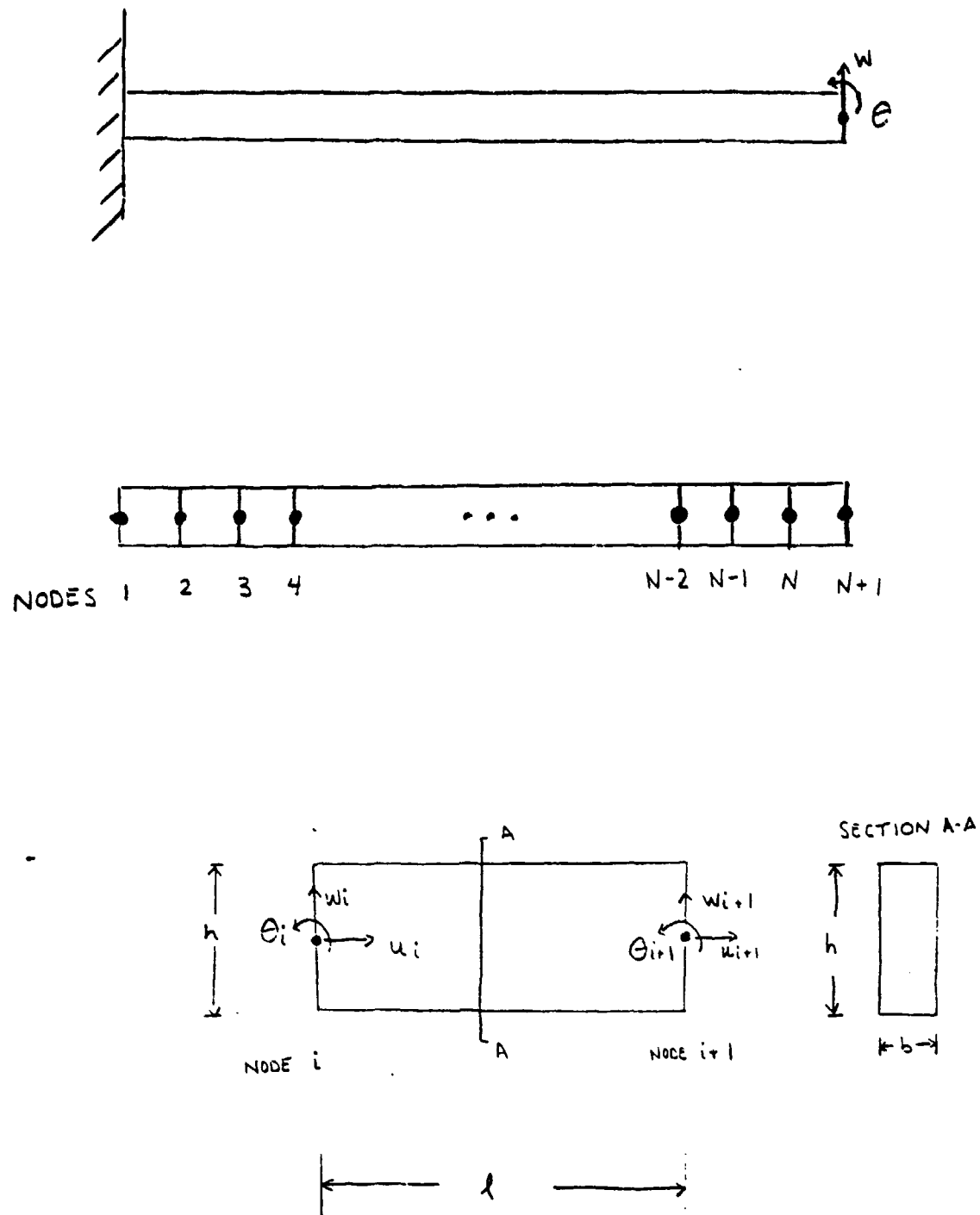


Figure 3 Cantilever Beam, Discretized Model, and Beam Element

## Boundary Conditions

$$w_1 = 0$$

$$\theta_1 = 0$$

Because the beam is cantilevered, the boundary conditions at the wall are zero transverse displacement ( $w_1 = 0$ ) and zero rotational displacement ( $\theta_1 = 0$ ). The effect of these boundary conditions, when the problem is split into known and unknown displacements as discussed earlier, is to reduce the order of the set of equations by 2. Body, surface, and initial stresses are assumed to be zero in this model. SatCon actuators will provide concentrated control forces to the beam. Thus the concentrated force vector  $R$  is dependent on the number and nodal location of the actuators.

As explained previously, the usual method for defining stiffness and mass matrices involves choosing interpolations to relate displacements within the element to displacements of the nodes. In the model used for this study, the element stiffness and mass matrices were derived using the "exact" displacements obtained by solving the static beam Equations (15) and (16)<sup>12</sup>.

Axial Behavior:

$$\frac{d}{dx} \left( EA \frac{du}{dx} \right) = 0 \quad (15)$$

$x$  = distance along element  $i$  and

$E$  = Young's Modulus

$A$  =  $bh$

$u(x = 0) = u(\text{NODE } i)$

$$u(x = 1) = u(\text{NODE } i+1)$$

$$u(x, y) = u(x) - y\theta(x)$$

Bending Behavior:

$$\frac{d^2}{dx^2} (EI \frac{d^2 w}{dx^2}) = 0 \quad (16)$$

$$w(x = 0) = w(\text{NODE } i+1) \text{ and } w(x = 1) = w(\text{NODE } i+1)$$

$$I = \text{Moment of Inertia} = bh^3/12 \text{ (see Figure 3)}$$

The element stiffness and mass matrices (neglecting axial behavior) are shown in Figure 4 (The structure of the stiffness and mass matrices which incorporate axial behavior is such that the transverse displacement,  $w$ , and the rotational displacement,  $\theta$ , do not depend on the axial displacement,  $u$ ). The stiffness and mass matrices for the whole structure are obtained by adding together the appropriate matrices of all the elements.

To transform to a first order finite state set of equations needed for the control software, a new state vector (which neglects axial behavior) is defined and Equation (14) is rewritten as:

$$\begin{bmatrix} \dot{U} \\ U \end{bmatrix} = \begin{bmatrix} 0 & I \\ -M^{-1} K & 0 \end{bmatrix} \begin{bmatrix} U \\ \dot{U} \end{bmatrix} + \begin{bmatrix} 0 \\ M^{-1} \end{bmatrix} \begin{bmatrix} R \end{bmatrix} \quad (17)$$

$$U = [w_2 \ \theta_2 \ \dots \ w_{N+1} \ \theta_{N+1} \ w_2 \ \theta_2 \ \dots \ w_{N+1} \ \theta_{N+1}]^T$$

Equation (17) includes the effect of the boundary conditions of zero displacement and rotation at the wall.

$$K^m = \frac{E b^3}{1-\nu^2}$$

$$\begin{bmatrix} 3 & 3 & 3 & 3 \\ h & h & h & h \\ \frac{1}{2} & \frac{1}{2} & \frac{1}{2} & \frac{1}{2} \\ 3 & 2 & 3 & 2 \\ 1 & 2 & 1 & 2 \\ 3 & 3 & 3 & 3 \\ h & h & h & h \\ \frac{1}{2} & \frac{1}{2} & \frac{1}{2} & \frac{1}{2} \\ 2 & 3 & 2 & 6 \\ 2 & 1 & 2 & 1 \\ 3 & 3 & 3 & 3 \\ h & h & h & h \\ \frac{1}{2} & \frac{1}{2} & \frac{1}{2} & \frac{1}{2} \\ 3 & 2 & 3 & 2 \\ 1 & 2 & 1 & 2 \\ 3 & 3 & 3 & 3 \\ h & h & h & h \\ \frac{1}{2} & \frac{1}{2} & \frac{1}{2} & \frac{1}{2} \\ 2 & 6 & 2 & 3 \\ 2 & 1 & 2 & 1 \end{bmatrix}$$

(a) Element Stiffness Matrix

$$M^m = b e$$

$$\begin{bmatrix} \frac{26 h^3 + 7 h^3}{70 l} & \frac{44 h^3 + 7 h^3}{840} & \frac{9 h^3 - 7 h^3}{70 l} & -\frac{26 h^3 - 7 h^3}{840} \\ \frac{44 h^3 + 7 h^3}{840} & \frac{6 h^3 + 7 h^3 l}{630} & \frac{26 h^3 - 7 h^3}{840} & -\frac{18 h^3 + 7 h^3 l}{2520} \\ \frac{9 h^3 - 7 h^3}{70 l} & \frac{26 h^3 - 7 h^3}{840} & \frac{26 h^3 + 7 h^3}{70 l} & -\frac{44 h^3 + 7 h^3}{840} \\ -\frac{26 h^3 - 7 h^3}{840} & \frac{18 h^3 + 7 h^3 l}{2520} & -\frac{44 h^3 + 7 h^3}{840} & \frac{6 h^3 + 7 h^3 l}{630} \end{bmatrix}$$

(b) Element Mass Matrix

Figure 4

### Dynamic Characteristics of the Beam Model

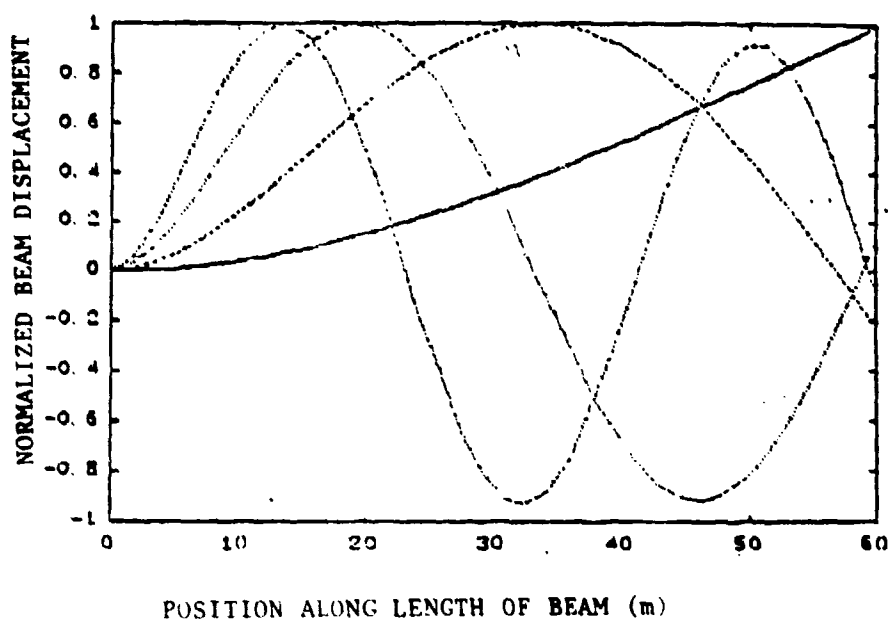
The beam model used in this study could be a simplified model for a variety of flexible structures, such as a robotic arm or a deployable truss structure. The beam model chosen is a mathematical representation of the MAST space structure (Figure 1). A beam of length 60 m (197 ft) with a lowest natural frequency of 1.15 rad/sec (0.184 Hz) was chosen for this analysis. To obtain these values, the physical parameters used are displayed in Table 1. A 247 kg mass (544 lbm) with a moment of inertia of 20 kg m<sup>2</sup> (475 lbm ft<sup>2</sup>) was situated at the tip of this model<sup>13</sup>. A 35 element model was used in the calculation of natural frequencies (Table 2) and mode shapes. Figure 5 is a plot of the first four mode shapes. The lowest mode in this plot has a large transverse deflection at the tip. As the excitation frequencies get higher, more energy is required to move the large tip mass and the tip increasingly behaves like a pinned end.

Table 1. Physical Parameters of Beam Model

|        |   |                 |   |                                    |                              |
|--------|---|-----------------|---|------------------------------------|------------------------------|
| E      | = | Young's Modulus | = | $5.2 \times 10^7$ N/m <sup>2</sup> | (7542 psi)                   |
| $\nu$  | = | Poisson's Ratio | = | 0                                  |                              |
| h      | = | Beam Height     | = | 1.7 m                              | (5.6 ft)                     |
| b      | = | Beam Width      | = | 1.42 m                             | (4.66 ft)                    |
| L      | = | Beam Length     | = | 60 m                               | (197 ft)                     |
| $\rho$ | = | Mass Density    | = | 1.95 Kg/m <sup>3</sup>             | (0.122 lbm/ft <sup>3</sup> ) |

**Table 2. Lowest Four Natural Frequencies of  
35 Element Model.**

0.184 Hz  
1.83 Hz  
5.7 Hz  
11.7 Hz



**Figure 5 Mode Shapes**

## ACTUATOR DESIGN

This section is a discussion of the actuator design concepts which were investigated. Because many of the actuator designs involve the production of forces and torques by interacting currents, the first part of the section is a review of the electromagnetic analysis methods. The next section describes the five actuator approaches examined and discusses some of the advantages and disadvantages associated with each particular approach.

### Magnetic Analysis Methods

#### Magnetic Forces

Circuits carrying electrical current produce forces on each other. For the general case depicted in Figure 6, this force can be obtained by the magnetic force law

$$F_{ab} = \left( \frac{\mu_0}{4\pi} \right) I_a I_b \oint_a \oint_b \frac{1}{r^2} d\mathbf{l}_b \times (\mathbf{r}_{ab} \times d\mathbf{l}_a) \quad (18)$$

where  $F_{ab}$  is the force exerted by current  $I_a$  on current  $I_b$ . The line integrals are evaluated over the two circuits, and the vectors  $d\mathbf{l}_a$  and  $d\mathbf{l}_b$  are incremental elements which point in the direction of the current flow. The constant  $\mu_0 = 4\pi \times 10^{-7} \text{ N/A}^2$  ( $8.99 \times 10^{-8} \text{ lb/A}^2$ ) is the permeability of free space<sup>14</sup>. The magnetic force can be written another way so that it is more obvious that Newton's third law holds.

In general these integrals cannot be evaluated analytically. They are performed numerically. However by rewriting Equation (18), we can express the force  $F_{ab}$  as an interaction of the current "b" with the field of the current "a".

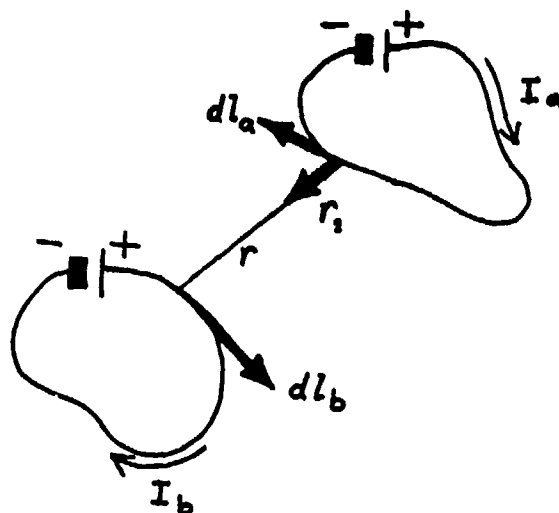


Figure 6 Two Current Loops

$$F_{ab} = I_b \oint dl_b \times B_a \quad (19)$$

where

$$B_a = \left( \frac{\mu_0}{4\pi} \right) I_a \oint_a \frac{1}{r^2} (dl_a \times r_1) \quad (20)$$

This is the Biot-Savart Law for the force between two current loops<sup>15</sup>.  $B_a$  is the magnetic induction due to circuit a at the position of element  $dl_{ab}$  and is measured in units of Tesla. This expression can be evaluated for simple geometries. The flux of the magnetic induction through a surface S is defined by<sup>16</sup>

$$\Phi = \int_S B \cdot dA \quad (21)$$

Another method can be used to calculate the force exerted on circuit "a" due to circuit "b". This method is based on energy

methods. By assuming a small virtual translation of one coil and then using the conservation of energy, the magnetic force in any direction  $x$  can be written as

$$F_{ab} = I_a I_b \left( \frac{\partial M}{\partial x} \right) \quad (22)$$

where  $M$  is the mutual inductance between the two circuits and can be related to the magnetic flux linking the circuits<sup>17</sup>:

$$\Phi_{ba} = M I_b \quad (23)$$

In physical situations, these interacting circuits which produce force on one another are made up of coils of wire and can thus be referred to as coils.

#### Far-Field Approximation

At distances which are large compared to the size of a coil (i.e., at least 10 coil radii away), far field approximations can be made for the magnetic induction and the interaction force. In this case, the magnetic field can be described using spherical coordinates  $r, \theta, \phi$  for a coil located at the origin (Figure 7)<sup>18</sup>.

$$\begin{aligned} B_r &= \left( \frac{\mu_0 2m}{4\pi r^3} \right) \cos \theta \\ B_\theta &= \left( \frac{\mu_0 m}{4\pi r^3} \right) \sin \theta \\ B_\phi &= 0 \end{aligned} \quad (24)$$

where  $\mathbf{m} = IS\mathbf{n}$  is the magnetic dipole moment of the current loop and  $\mathbf{n}$  is a unit vector perpendicular to the plane of the coil. Because field falls off as the cube of the distance from the origin  $r^3$ , placing a second interacting coil closer to the origin

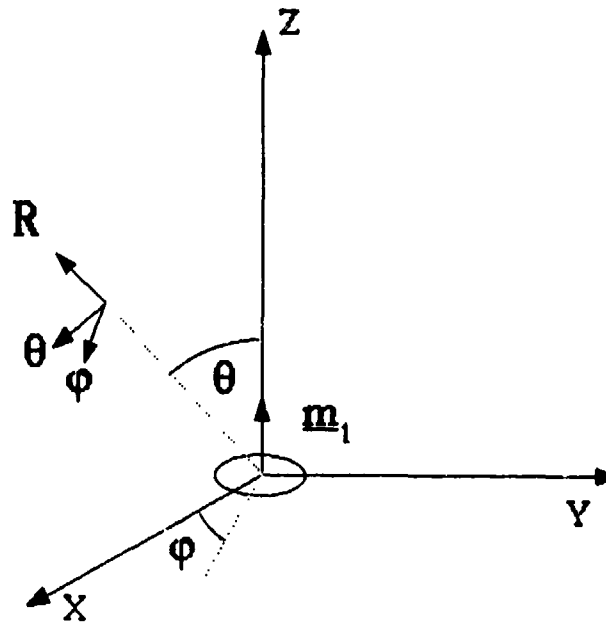


Figure 7 Spherical Coordinate System

will produce stronger interaction forces and torques. The interaction force and torque due to coil 1 located at the origin with its magnetic moment in the z direction on coil 2 located at  $(R, \theta, \phi)$  (see Figure 8) can be written as below<sup>19</sup>

$$\mathbf{F} = \mathbf{m}_2 \nabla (\mathbf{B}_1 \cdot \mathbf{m}_2) = (\mathbf{m}_2 \cdot \nabla) \mathbf{B}_1 \quad (25)$$

$$\mathbf{\tau} = \mathbf{m}_2 \times \mathbf{B}_1 \quad (26)$$

Notice that the interaction force is a function of the gradient of the magnetic field and therefore is proportional to the inverse of the fourth power of the separation distance ( $F \propto 1/r^4$ ). The torque, on the other hand, is proportional to the inverse of the third power of the separation distance ( $\tau \propto 1/r^3$ ). Thus the strength of the force falls off more quickly with distance than does the strength of the torque. Because we are considering actuation schemes which involve both force and torque

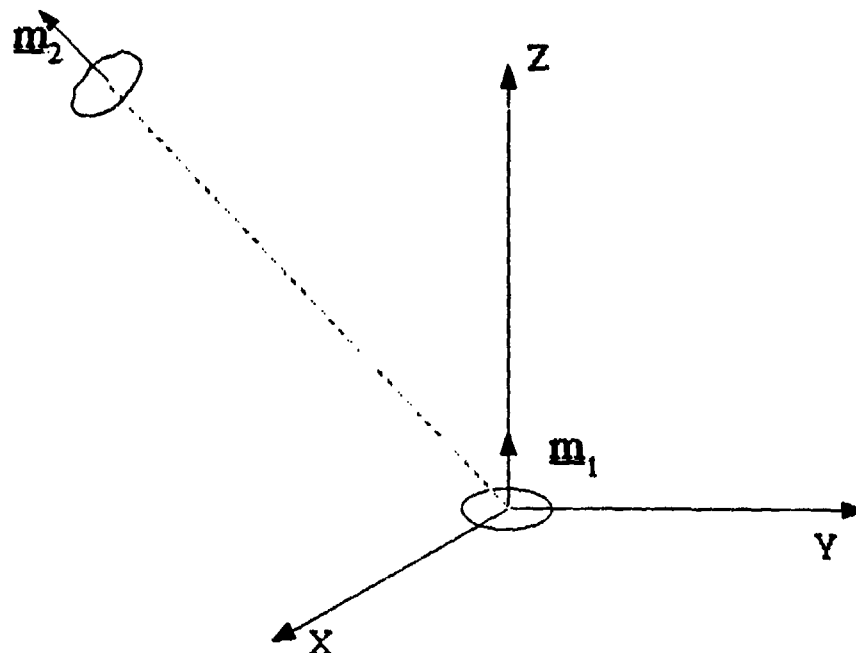


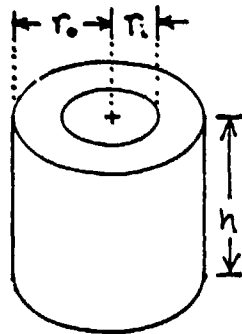
Figure 8 Two Interacting Dipoles

capability and these capabilities are sometimes traded off in the design process, this fact will have important implications regarding the actuator effectiveness. When the far field approximation is used, the coils are sometimes referred as dipoles.

#### Example "Standard" Dipole

Most of the actuator approaches examined will use control coils. The remainder of this report will make extensive use of a "standard size" control coil for scaling analysis. This "standard" coil, shown in Figure 9, has an outer radius ( $r_o$ ) of 5

cm (1.97 in), an inner radius ( $r_i$ ) of 2.5 cm (0.98 in), a height ( $h$ ) of 10 cm (3.94 in) and a current density ( $J$ ) of  $10^6$  A/m<sup>2</sup> (645 A/in<sup>2</sup>). This current density is very conservative, typical of household wiring. For reference purposes, the volume of this coil is 589 cm<sup>3</sup> (35.9 in<sup>3</sup>), and its mass is 1.6 kg (3.5 lbm) if made of aluminum.



$$r_o = 0.05 \text{ m}$$

$$r_i = 0.025 \text{ m}$$

$$h = 0.1 \text{ m}$$

$$J = 10^6 \text{ A/m}^2$$

Figure 9 "Standard" Size Coil

The magnetic moment of the "standard" dipole can be calculated using Equation (27).

$$\mathbf{M} = 0.5 \int \mathbf{r} \times \mathbf{J} dV = \pi h J (r_o^3 - r_i^3) = 11.4 \text{ A m}^2 \text{ (123 A ft}^2\text{)} \quad (27)$$

The interaction force and torque between two of these "standard" dipoles can be calculated using Equation (25) and (26). For a configuration shown in Figure 10, in which the dipole moments are perpendicular to each other, and a coil separation distance of 1 m (3.28 ft) the resulting force and torque on coil 2 are

$$\mathbf{F} = \frac{3}{4} \frac{\mu_o |\mathbf{M}_1| |\mathbf{M}_2|}{\pi r^4} \mathbf{x} = 3.9 \times 10^{-5} \text{ N (} 8.8 \times 10^{-6} \text{ lb)} \mathbf{x} \quad (28)$$

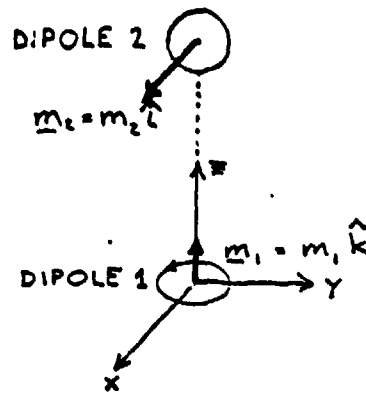


Figure 10 Configuration for Example Calculations of Interaction Force and Torque on Two Standard Size Coils

$$F = - \frac{\mu_0 |M_1| |M_2|}{2\pi r^3} \hat{y} = 2.6 \times 10^{-5} \text{ N m} (1.9 \times 10^{-5} \text{ ft lb}) \hat{y} \quad (29)$$

Note that for this example configuration, the force and torque are perpendicular both to each other and to the axis connecting the coils. Importantly, a system containing both dipoles will see no net force or torque, although each dipole experiences both torque and force. The equilibrium of a system containing both dipoles is a direct consequence of Newton's third law. The force and torque on coil 1 can be found using Newton's third law. For example, the force on coil 1 is equal in magnitude and opposite in direction to the force on coil 2 by force equilibrium.

#### Maxwell's Mutual Inductance Formula for Circular Filaments

When the dipole approximation can not be used, another method must be used to obtain the interaction forces.

For two equal radius circular filaments coaxially located as shown in Figure 11, the mutual inductance can be expressed in a formula given by Maxwell<sup>20</sup>:

$$M = 4 \pi a \left( \left( \frac{2}{k} - k \right) F - \frac{2}{k} E \right) \quad (30)$$

where

$$k = 2 / \sqrt{1 + (r^2/a^2)}$$

$a$  = radius of circular filaments

$r$  = distance between centers of filaments

$F$  = Complete elliptic integral of the first kind with respect to modulus  $k$

$E$  = Complete elliptic integral of the second kind with respect to modulus  $k$

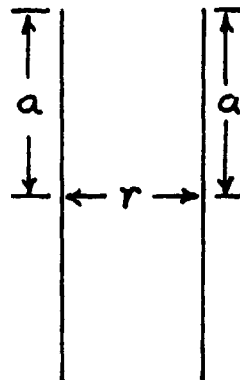


Figure 11 Two Coaxial Equal-radius Circular Filaments

By differentiating this expression with respect to  $r$  and multiplying by the products of the currents, as in Equation (22), an expression for the force can be written. This differentiation can be performed numerically by using the polynomial approximations for the elliptic integrals found in Reference 21. It turns out that the interaction force between the two current loops is a function of the ratio of the separation distance to the coil radius ( $r/a$ ). The magnitude of the force normalized by

the product of currents is shown in Figure 12. This plot shows that at near field ( $r/a < 1$ ) the filament force is inversely proportional to  $r/a$ . For far field ( $r/a > 10$ ), the force goes as the negative fourth power of  $r/a$ . This can be verified using the dipole far field approximations for force as shown earlier.

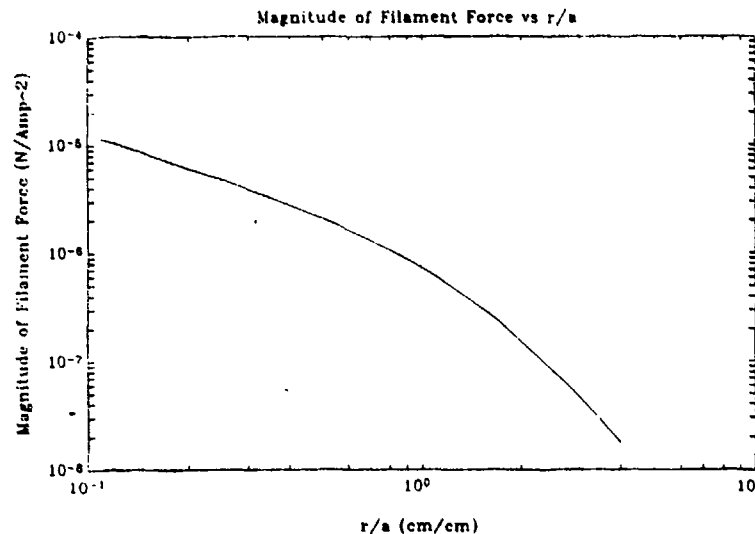


Figure 12 Near Field Filament Interaction Force

#### ACTUATOR APPROACHES

This section describes the actuator design approaches examined in this study. Most of these designs involve the interaction of a magnetic coil with a magnetic field from another source. Hence the actuator designs are based on the analysis developed in the previous section. The first actuator design uses a number of distributed coils at various places in the flexible structure that interact with the Earth's magnetic field to produce control torques. The second design approach uses a large magnetic flux source and produce torques on the structure by interaction of distributed coils and this flux source. The

third design approach produces forces and torques on the structure by the interaction of distributed coils. The fourth design approach uses a local interaction scheme that involves placing coils close together on structural truss producing force or strain that is transmitted to the overall beam structure. The final approach involves the use of a magnetostrictive material in order to control the structure.

#### Interaction of Distributed Coils with Earth's Magnetic Field

This actuator design uses magnetic coils distributed along the structure interacting with the Earth's magnetic field and producing control torques on the structure. This actuator concept is illustrated schematically in Figure 13.

The Earth's magnetic field can be modelled as that of a dipole. The magnitude of this field can change for a variety of reasons. Solar wind, solar radiation and sunspots, for example, can alter the field's strength. The dipole strength is decreasing by 0.05% per year<sup>22</sup>. The field intensity also varies with longitude, latitude, and altitude. The variation of the maximum value of the Earth's magnetic field with altitude is shown in Figure 14. Notice that as can be expected from the far-field equations for magnetic strength of a dipole (Equation (24)), the strength of the field decreases with altitude. Altitudes typical of low-Earth-orbit applications are 50 km. This includes space shuttle applications such as MAST. At this altitude the magnetic field strength is on the order of 0.5 Gauss ( 50 microtesla). This field strength will be used in

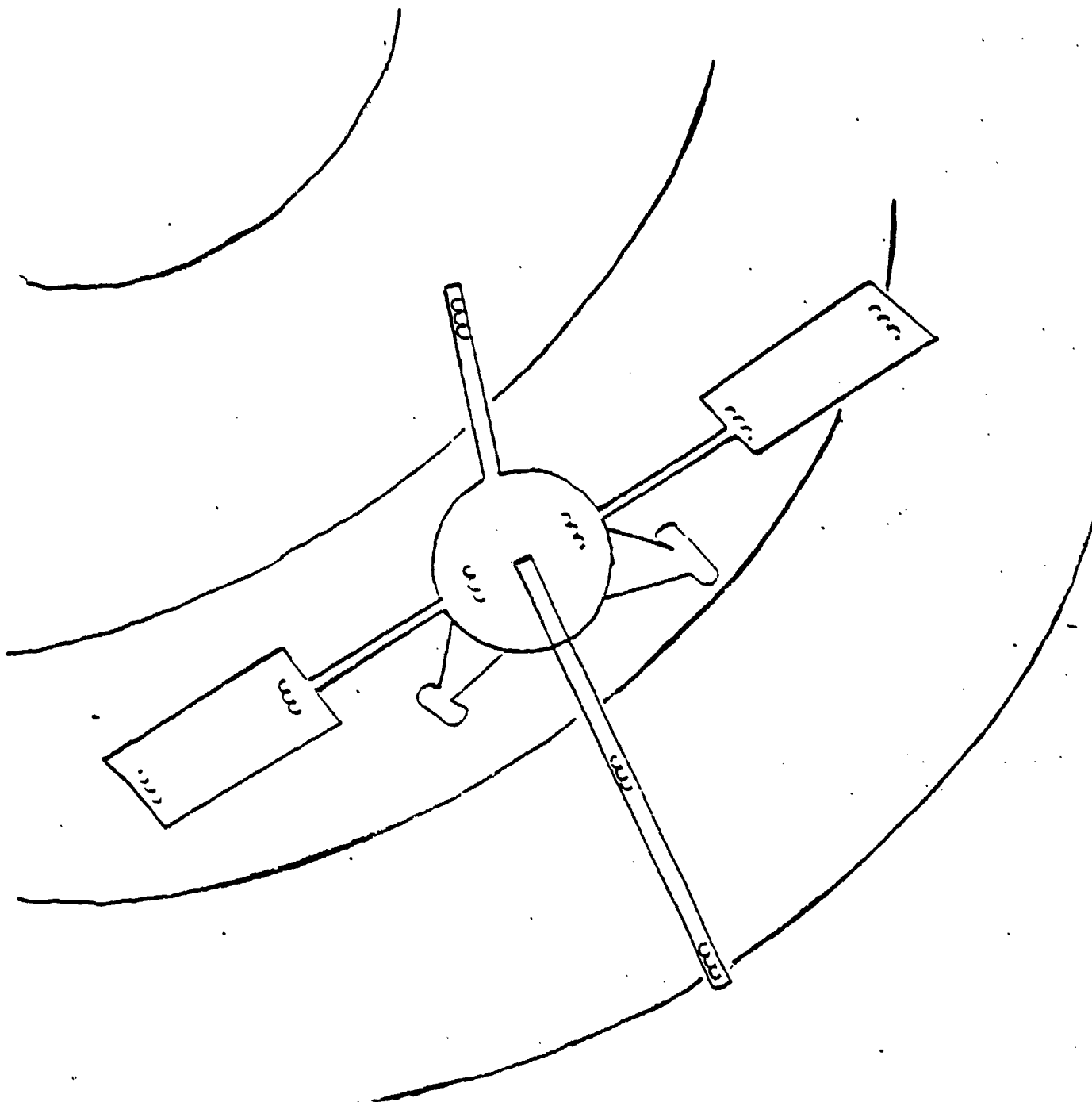


Figure 13 Actuator Approach 1: Interaction of Distributed Coils with Earth's Magnetic Field

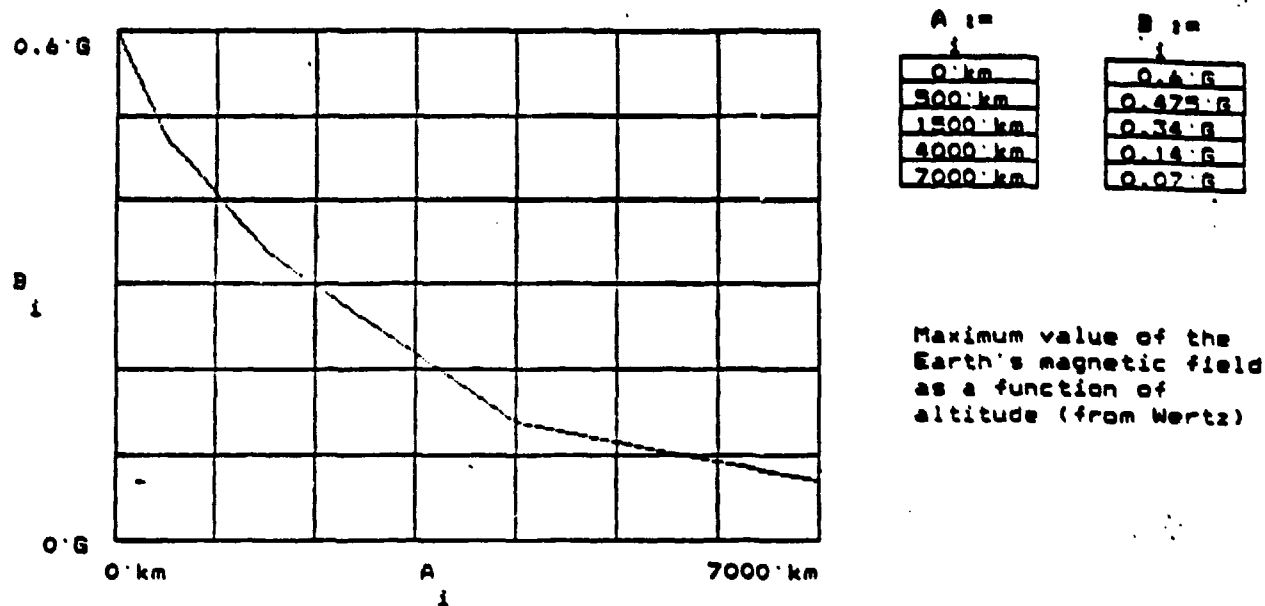


Figure 14 Earth's Magnetic Field vs Altitude

the calculations that follow.

Because the Earth's magnetic field is relatively constant (i.e., the gradient is very small), this actuation system is not good at producing control forces on the structure. This is because the dipole force is proportional to the gradient of the magnetic field (Equation 25). The control torques on the structure, on the other hand, can be calculated from Equation (26). The maximum torque that this technique can produce was

calculated by using a relatively large control dipole and assuming an orientation relative to the Earth's magnetic field which maximizes the torque. A "standard" size control dipole of (Figure 9) was used to calculate the torque available at an altitude typical for low-Earth-orbit space applications (such as the shuttle). At this altitude, the earth's magnetic field is 50 microtesla (0.5 Gauss). The resulting torque and torque per unit of actuator mass are presented below.

$$\tau = 5.7 \times 10^{-4} \text{ Nm} \quad (4.2 \times 10^{-4} \text{ ft lb}) \quad (31)$$

$$\frac{\tau}{\text{mass}} = 3.5 \times 10^{-4} \frac{\text{Nm}}{\text{Kg}} \quad (1.2 \times 10^{-4} \text{ ft lb/lbm})$$

These torques are rather small for controlling the beam model used in this study. Another disadvantage of this actuator design for control of the MAST model is its dependence on the orientation of the actuator to the Earth's magnetic field. A control system which incorporates these actuators for shape and vibration control would have to sense and control positioning of the actuator with respect to inertial space.

#### Interaction of Distributed Coils with a Large Flux Source

This actuator design concept is similar to the above except that instead of the Earth's magnetic field, a large flux source is mounted on the spacecraft. The field produced by this flux source interacts with distributed coils and produces control torques. A schematic of this approach is shown in Figure 15.

A superconducting solenoid with a current density of  $10^5 \text{ A/m}^2$  ( $9.3 \times 10^6 \text{ A/ft}^2$ ) magnetic moment of  $10^7 \text{ Am}^2$  ( $1 \times 10^8 \text{ A ft}^2$ )

was used as the baseline flux source. The dimensions of this solenoid are shown in Figure 16. This is a large solenoid. Its height ( $h$ ) is 1 m (3.3 ft) and its outer radius ( $r_o$ ) is 0.5 m (1.6 ft). Its volume is  $0.6 \text{ m}^3$  ( $21 \text{ ft}^3$ ) and its mass is approximately 5200 kg ( $1.1 \times 10^4 \text{ lbm}$ ).

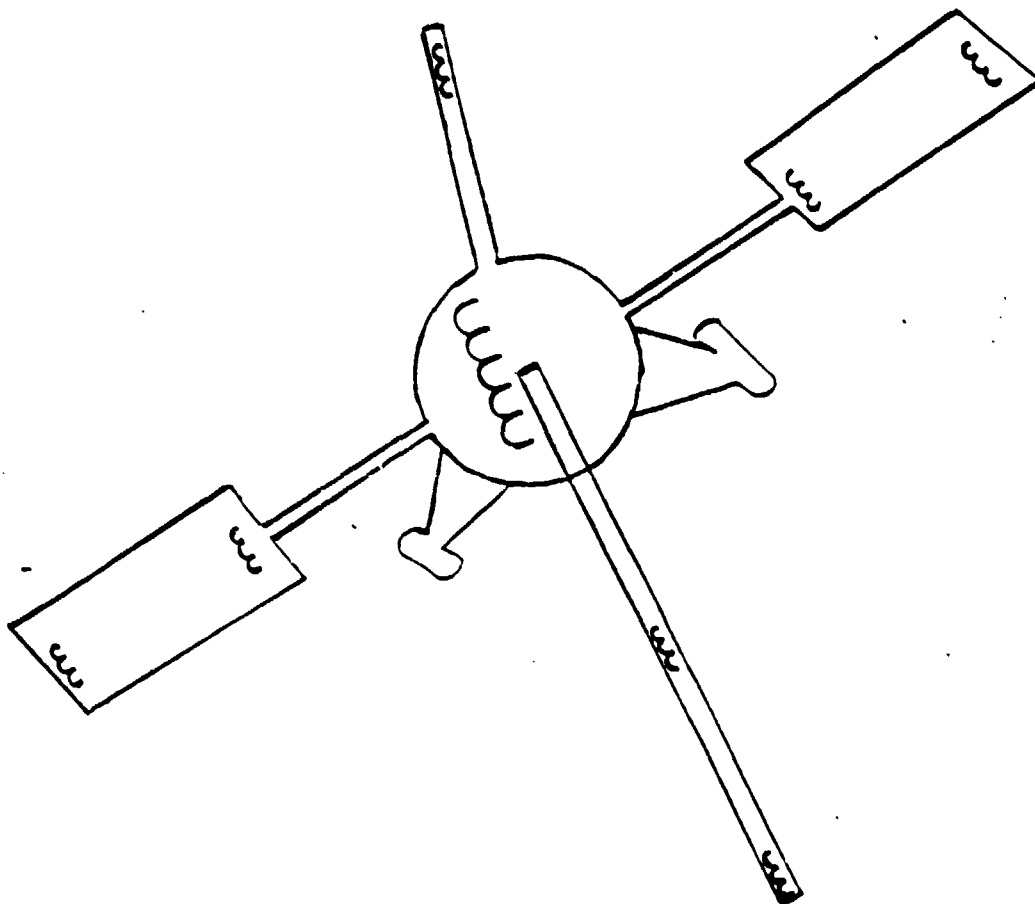
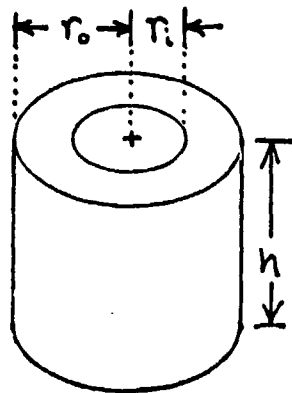


Figure 15 Actuator Approach 2: Interaction of Distributed Coils with Large Flux Source



$$\begin{aligned} r_o &= 0.5 \text{ m} \\ r_i &= 0.25 \text{ m} \\ h &= 1 \text{ m} \\ J &= 10^8 \text{ A/m}^2 \end{aligned}$$

Figure 16 Large Flux Source Solenoid Dimensions

At a distance of 50 m (164 ft), the maximum torque on the "standard" size dipole (Figure 9) is  $1.05 \times 10^{-4}$  Nm ( $8 \times 10^{-5}$  ft lb). As in the previous actuator approach, this torque is dependent on the orientation of the control dipole with respect to the large flux source. The disadvantage of this approach is that torques can only be produced in two directions. This is clear from the dipole equation for torque (Equation (26)) which states that the torque goes as the cross product of the magnetic moment and the magnetic field; thus, torque cannot be produced in a direction which is parallel to the magnetic moment of the large flux source. Another disadvantage for application of these actuators to the MAST structure is that the large flux source experiences a large torque due to the Earth's magnetic field. This torque is about 570 Nm (420 ft lb) at an altitude place when the Earth's magnetic field strength is 50 microtesla (0.5 Gauss) (i.e., an altitude typical for low-Earth-orbit shuttle applications). Because MAST is designed to be deployed from the

shuttle payload bay, this torque would have to be carried by the shuttle. Flexible structure control of the MAST beam would have to be coupled with attitude control of the shuttle in order for this actuation scheme to be used. Thus this actuator approach is not desirable for the MAST application. This scheme, on the other hand, may be more advantageously employed for another type of spacecraft that combines attitude control with flexible structure control. In any case, the large flux source would need to be superconducting for acceptable power consumption.

#### Interaction of Distributed Coils

This actuator design approach places a number of magnetic coils along the structure and obtains forces and torques by the dipole interaction that exists between them. A schematic of this approach is shown in Figure 17.

Three configurations are considered which encompass the spectrum of all possible configurations (i.e., a general configuration would be a linear combination of these three) (Figure 18). The first dipole is placed at the origin with its magnetic moment in the  $z$  direction, and the position of the second dipole is varied for the three different configurations. In the first configuration, the second dipole is offset from the first by a distance,  $r$ , along the  $y$  axis and has a magnetic moment in the  $z$  direction. In the second configuration, the second dipole is offset a distance  $r$  along the  $z$  axis and its magnetic moment is in the  $x$  direction. The third configuration has the second dipole on the  $z$  axis as well, but with the

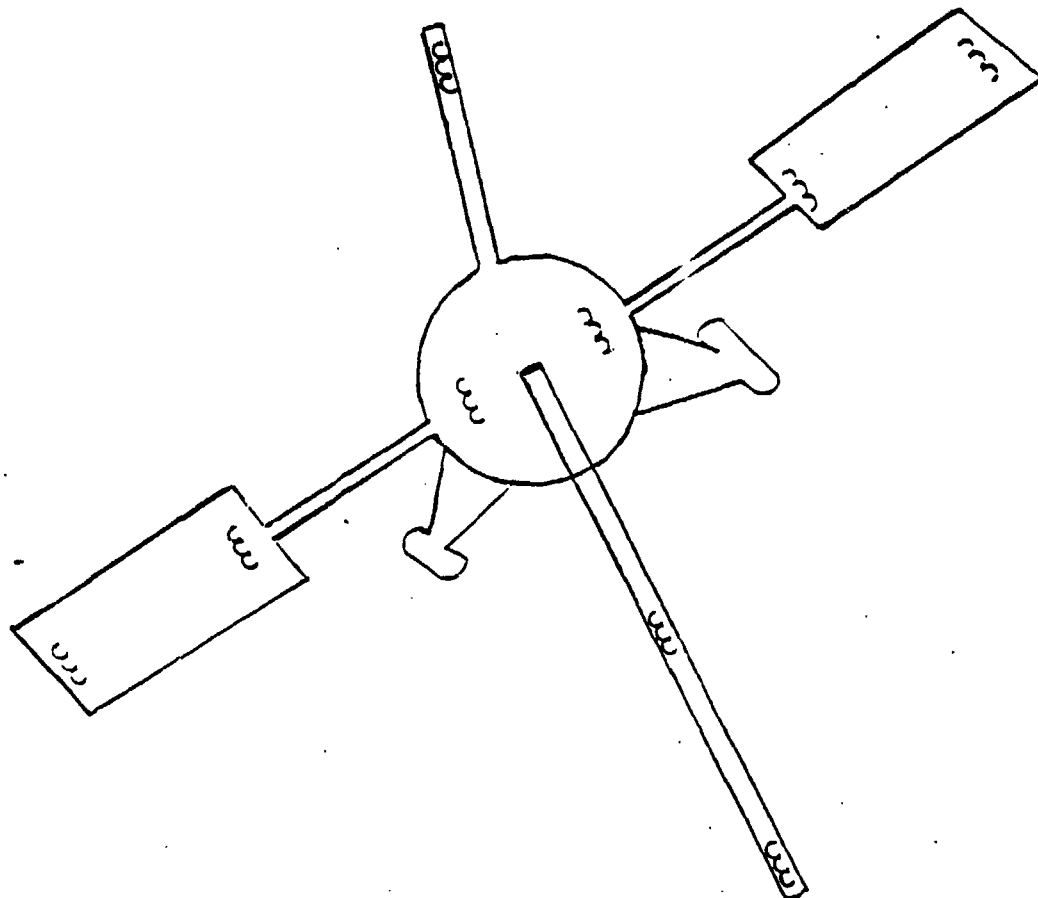
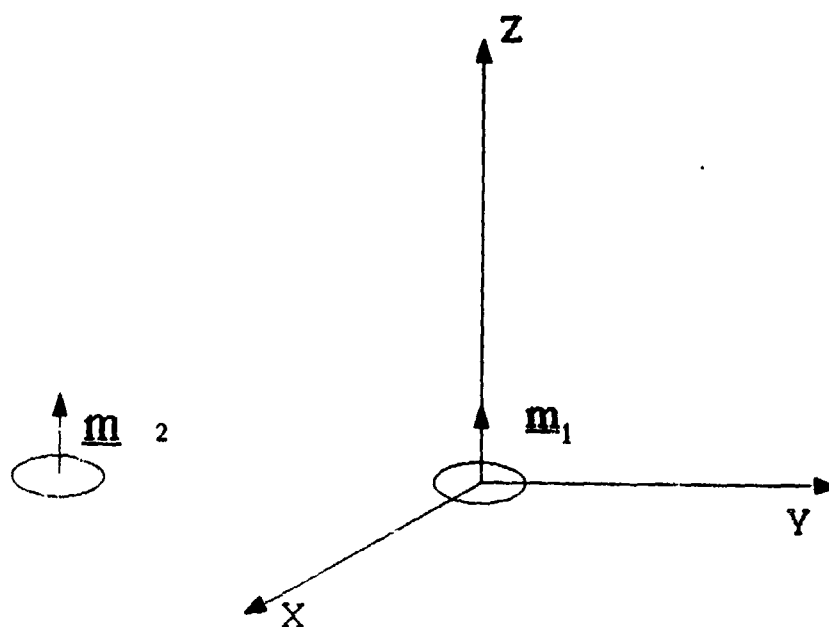


Figure 17 Actuator Approach 3: Interaction of Distributed Coils

magnetic moment in the  $z$  direction. The dipole forces and torques are computed as a function of magnetic moment using the far-field equations developed in the previous section (Equations (25) and (26)) and Newton's third law. The configurations and force/torque on coil 2 equations are shown in Figure 18. The force in all three configurations is proportional to  $1/r^4$  as expected from an earlier discussion about Equation (25). The force is strongest in the third configuration by a factor of 2. This configuration, however, has no torque capability. Only the second configuration is capable of producing both force and torque, as can be seen in the

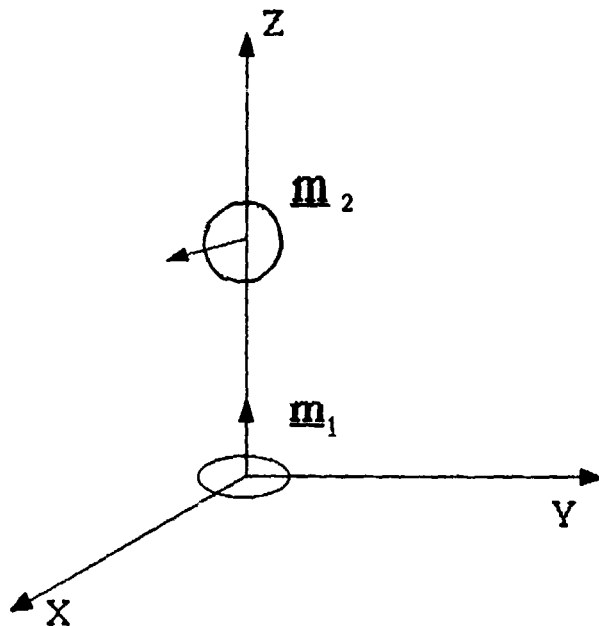
# Configuration 1



$$F = - \frac{3 \mu_0 m_1 m_2 Y}{4 \pi r^4} \quad r = 0$$

Figure 18(a) Configuration of Distributed Coils and Their Associated Dipole Interaction Force/Torque Expressions for Force/Torque on Coil 2

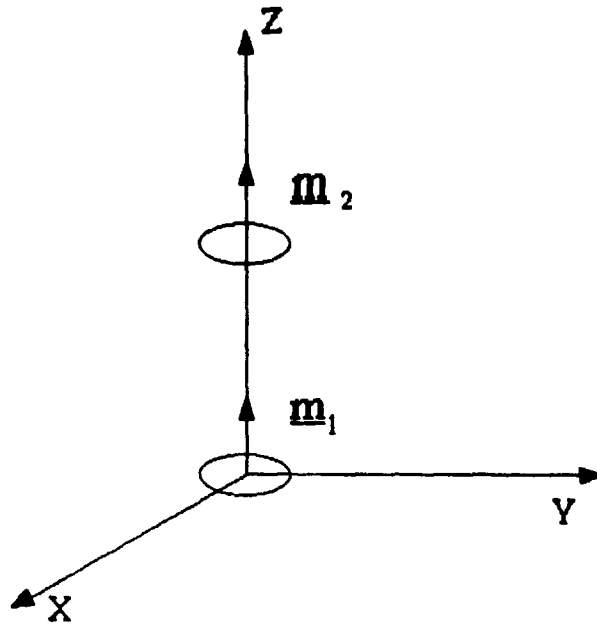
## Configuration 2



$$F = \frac{3 \mu_0 m_1 m_2}{4 \pi r^4} \quad \tau = - \frac{\mu_0 m_1 m_2}{2 \pi r^3} Y$$

Figure 18(b) Configuration of Distributed Coils and Their Associated Dipole Interaction Force/Torque Expressions for Force/Torque on Coil 2

### Configuration 3



$$\underline{F} = - \frac{3 \mu_0 \underline{m}_1 \underline{m}_2 \underline{z}}{2 \pi r^4} \quad \underline{\tau} = 0$$

Figure 18(c) Configuration of Distributed Coils and Their Associated Dipole Interaction Force/Torque Expressions for Force/Torque on Coil 2

equations in Figure 18. The magnitude of this torque is proportional to the inverse of the cube of the separation distance ( $\tau \propto 1/r^3$ ). This was also established earlier by consideration of the dipole Equation (26). The direction of the force and torque capability in the second configuration is appropriate for the control of beam bending behavior (Figure 19). This figure shows both the forces and the torques are in

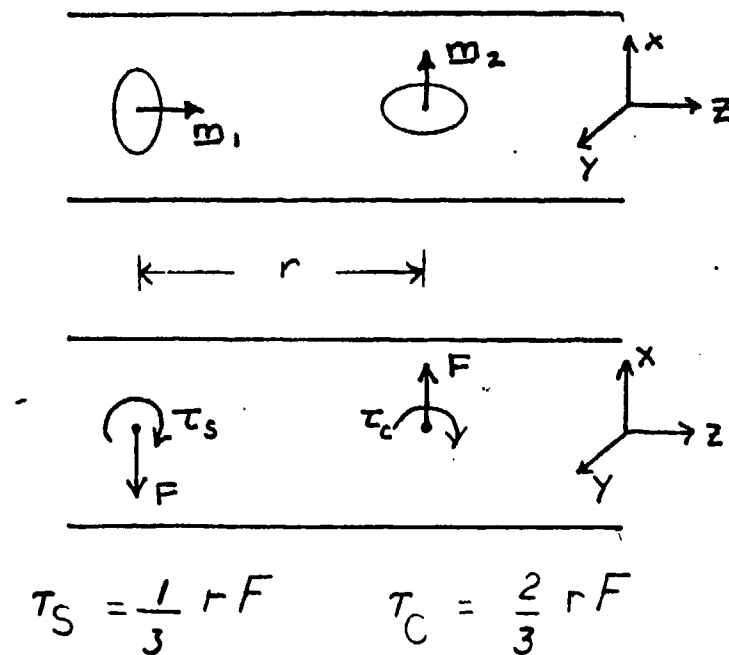


Figure 19 Configuration of Distributed Coils which Produces Both Force and Torques Suitable for Beam Bending Control

directions which support control of bending about the  $y$  axis. The sum of these forces and the sum of these torques is zero as can be expected from Newton's Third Law of Action-Reaction.

Calculations were performed to determine the magnitude of the force and torque capabilities as a function of separation distance,  $r$ , and current density,  $J$ . Figures 20, 21, and 22 are plots of coil 2 forces and torques normalized by the product of the magnetic moments of the two coils vs. dipole separation distance. These plots indicate the effect of separation distance. As established earlier by consideration of the dipole equations (Equations (24), (25), (26)), the strength of the force or torque

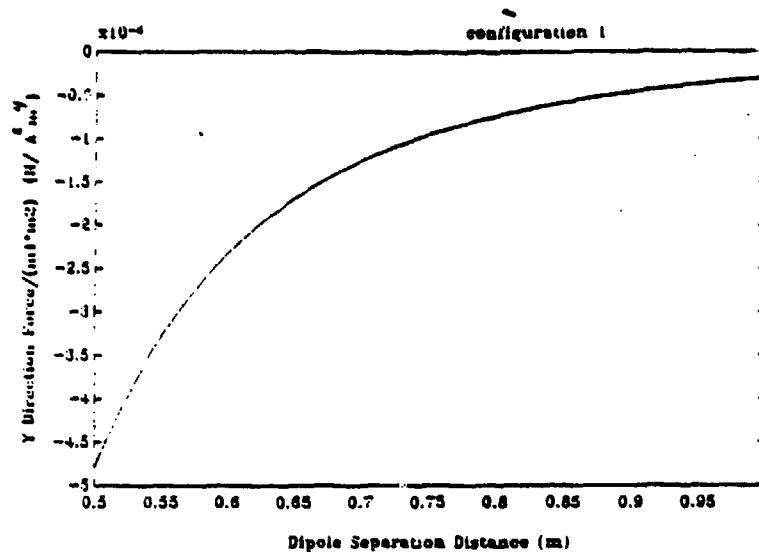


Figure 20 Force vs Separation Distance for Configuration

is weaker as the distance between the dipoles increases.

Comparison of these three configurations show that the force is strongest when the dipole moments are aligned with each other (the third configuration). If the dipoles have a magnetic dipole moment of  $11.4 \text{ A m}^2$  ( $123 \text{ A ft}^2$ ) as in the "standard" dipole, this force capability is on the order of  $10^{-4}$  Newtons ( $10^{-5} \text{ lb}$ ) for a separation distance of  $1/2 \text{ m}$  ( $1.6 \text{ ft}$ ). The other two configurations give forces that are half as strong for the same magnetic moments and separation distance. The second configuration, however, is the only one which is capable of producing a torque. This is significant as the torque falls off as  $1/r^3$  while the force falls off as  $1/r^4$  as shown earlier.

The effect of current density is shown in Figures 23, 24, and 25. Plotted is coil 2 force or torque vs current density.

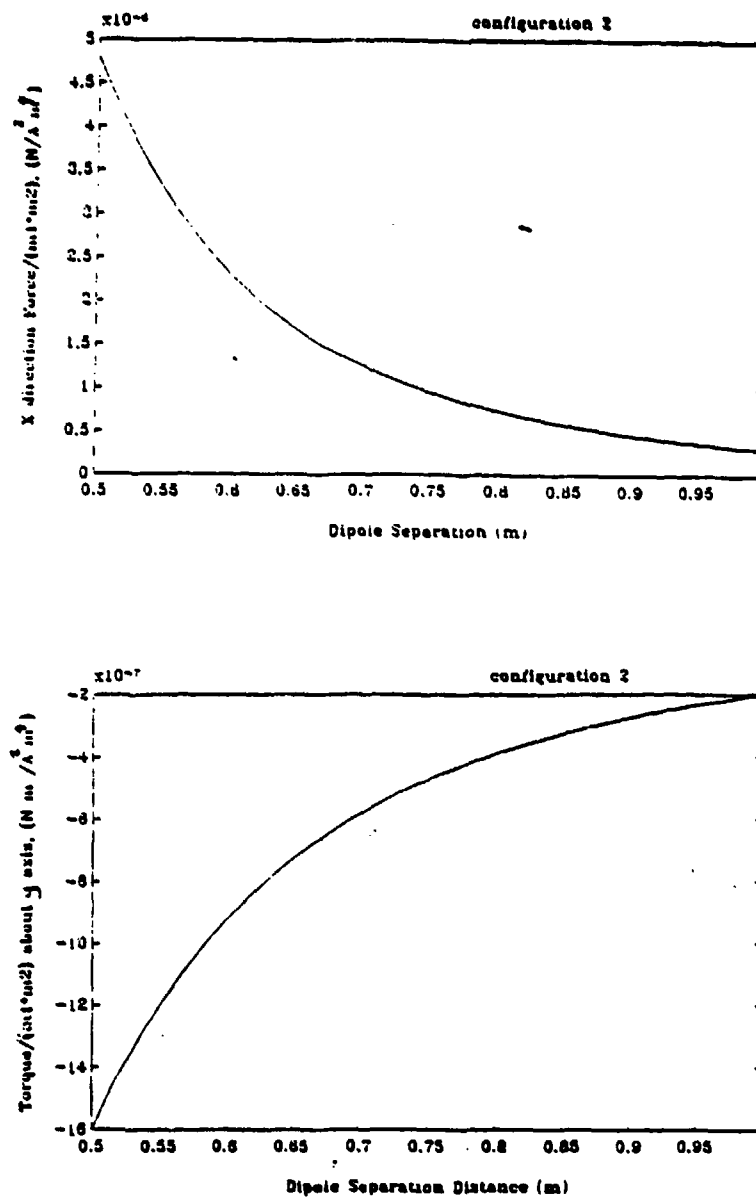
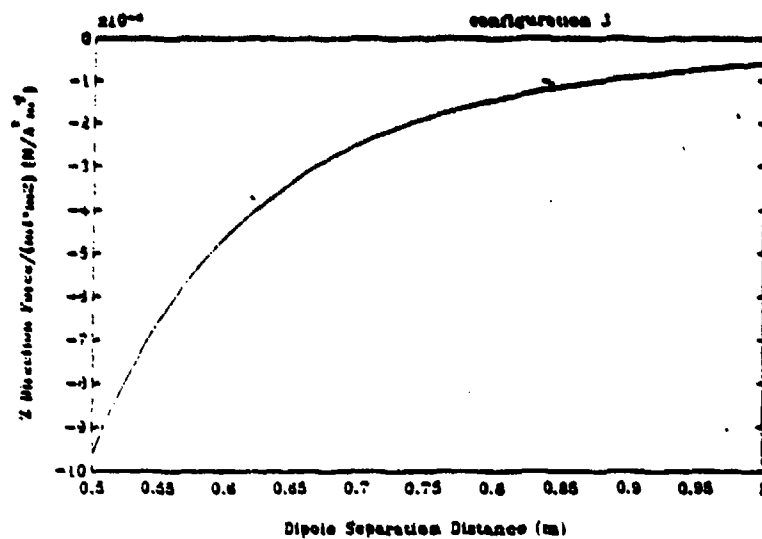
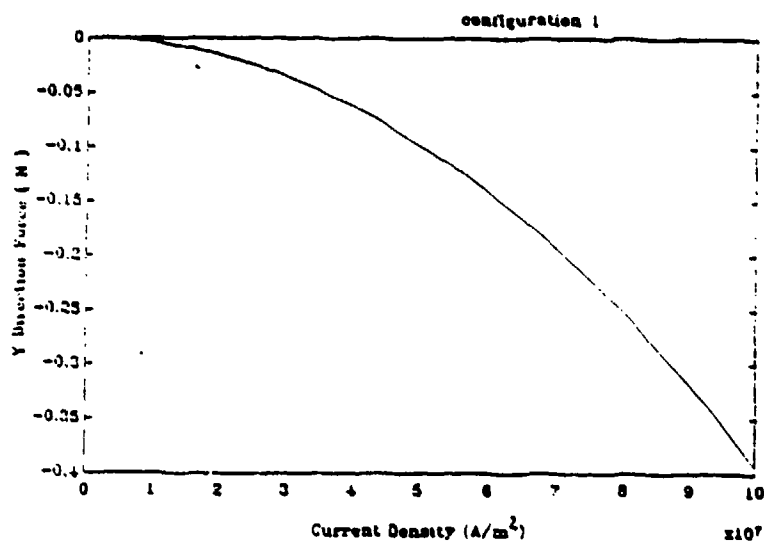


Figure 21 Force and Torque Separation Distance for Configuration 2



$$r = 0$$

Figure 22 Force vs Separation Distance for Configuration 3



$$r = 0$$

Figure 23 Force vs Current Density for Configuration 1

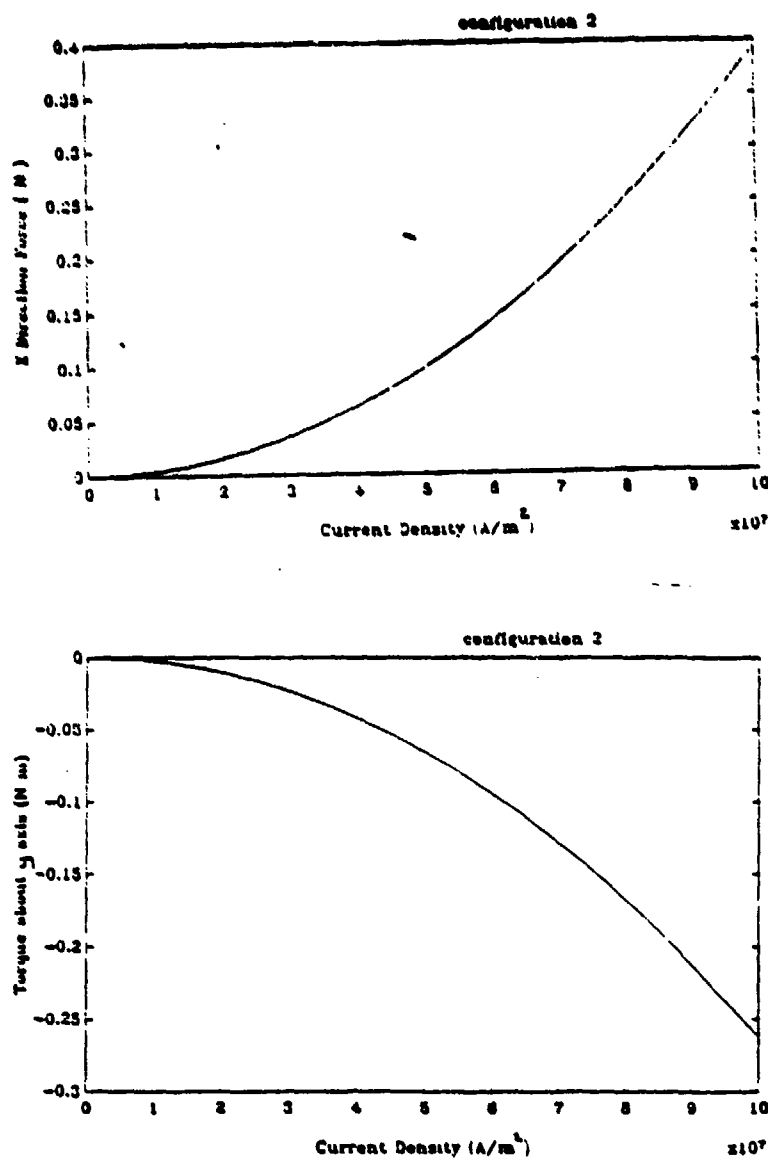
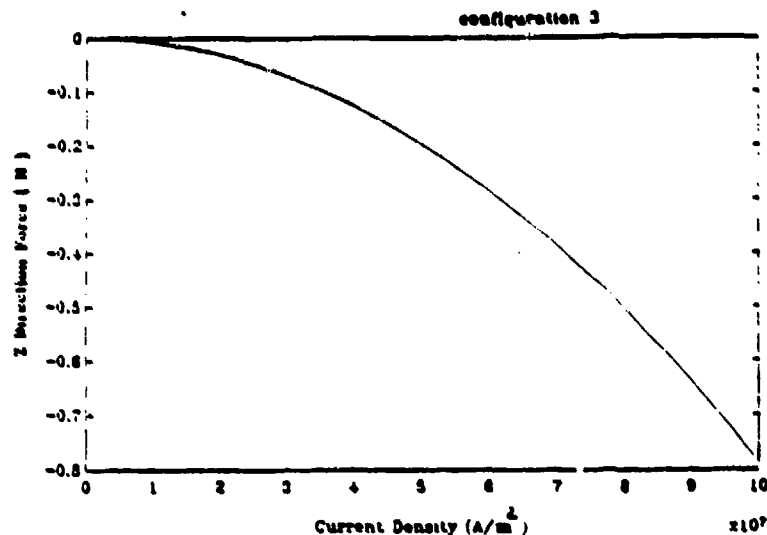


Figure 24 Force and Torque vs Current Density for Configuration 2

"Standard" size dipoles (Figure (9)) are used with a separation distance of 1 m (3.3 ft) ( $\mu = 11.4 \text{ Am}^2$  (123 A ft<sup>2</sup>)). Because the magnetic moment is proportional to the current density, the torques and forces are proportional to the square of the current density. Typical values of current density range from  $10^6 \text{ A/m}^2$  ( $9 \times 10^4 \text{ A/ft}^2$ ) in household wiring applications to  $10^8 \text{ A/m}^2$  ( $9 \times 10^6 \text{ A/ft}^2$ ) in superconductors. The plots show values on the order



$$\tau = 0$$

Figure 25 Force vs Current Density for Configuration 3

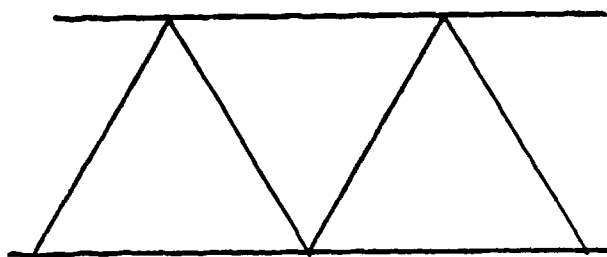
of 0.4 N (0.09 lb) and 0.25 Nm (0.18 ft lb) on coil 2 for the second configuration for a current density of  $10^8$  A/m<sup>2</sup> ( $9 \times 10^4$  A/ft<sup>2</sup>). The third configuration has a force which is twice as strong (0.8 N) (0.18 lb) for this current density but no torque. Claims of current densities of  $10^{10}$  A/m<sup>2</sup> ( $9 \times 10^8$  A/ft<sup>2</sup>) have been reported for new high-temperature superconductors, raising the force and torque potential of this actuator system by a factor of 10000.

Further investigation of the feasibility of this approach is provided in a following section.

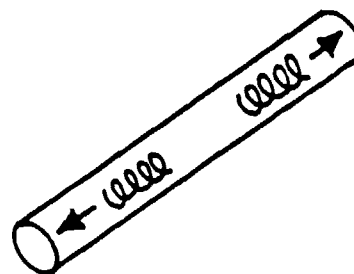
### Local Interaction of Magnetic Coils on a Truss Section

As established earlier, stronger forces and torques can be obtained by placing the coils closer together (Equations (25) and (26)). The fourth actuator approach is different from the previous concepts in that the coils are designed to be very close to each other to take advantage of the higher force capability.

This approach is to place magnetic coils on a truss section of the MAST beam model. A schematic of this approach is shown in Figure 26. Notice that these coils are in the configuration where their magnetic moments are aligned on the same axis. The dipole equations (Equations (25) and (26)) predict a force along this axis. This configuration is the same as configuration 3 in



BEAM WITH TRUSS SECTION



TRUSS SECTION

Figure 26 Actuator Approach 4: Local Coil Interaction

the previous discussion. However, unlike the previous actuator approach, the dipole equations (Equations (25) and (26)) can not be used in this approach because they break down at close separation distances ( $r < 10$  coil radii). Thus the alternate methods using Maxwell's mutual inductance formula (Equation (30)) will be necessary for the analysis.

In addition to more complicated methods to compute the coil force, the local interaction actuator approach requires more complicated modelling for the MAST beam-actuator interaction. As shown in Figure 27, there are two extreme ways to model this interaction with the beam. One way is as if the beam is much more massive than the truss and acts essentially as a kinematic constraint preventing motion. In this case, the force at the end of the truss is completely transmitted to the beam. If the coils are centrally located in the truss, and the truss is modelled as a continuous spring, the force transmitted to the beam is coil force reduced by a factor which is the ratio of the separation distance ( $r$ ) to the truss length ( $l$ ). Thus there is an inherent tradeoff between placing the coils close together to obtain a stronger magnetic force and placing them close to the end of the truss so that more force is transmitted to the overall beam structure.

In the other extreme model, the beam is assumed to deflect due to the magnetic coil interaction force. In this model, no force is transmitted to the beam. As emphasized in the Figure 27, the deflection of the beam under this modelling approximation

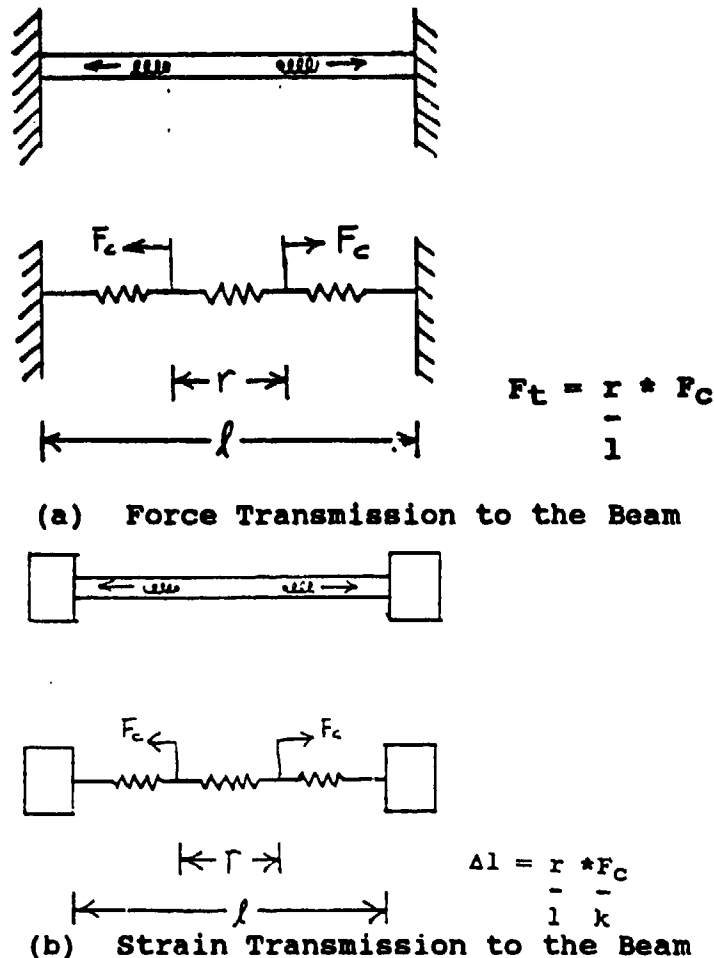


Figure 27 Extreme Models of Beam-Truss Interaction for Local Actuator Approach

is also proportional to the ratio of the separation distance ( $r$ ) to the truss length ( $l$ ). Thus the tradeoff between placing the coils close together and separating them is also in effect here. The two modelling extremes can be used to find two extreme approximations of what will actually happen. In actuality, there will be some force and some motion transmitted to the beam.

The advantage of the local interaction approach is that because the coils are closer together, they are able to produce a stronger force than the other type actuator designs. To analyze this approach, the near field calculation of the mutual

inductance in Maxwell's formula (Equation (30)) is necessary. This expression is then differentiated to find the interaction force (Equation (22)). As stated earlier, polynomial approximations for the elliptic integrals in the expression for mutual inductance and numerical differentiation was used to calculate the coil interaction force. The results were shown in Figure 12, a plot of force normalized by the product of the coil currents vs the ratio of coil separation to coil radius ( $r/a$ ). This plot can be used to find the magnitude of the force for given values of separation distance, coil radius, and coil currents.

An example calculation that is applicable to the MAST beam is included to illustrate this approach. For reference, some MAST trusses have a diameter of approximately 2.54 cm (1 inch). This value is used for the diameter of two coils centered in such a truss in a configuration so that their magnetic moments are aligned with the axis of the truss as in Figure 26. The coils are assumed to be separated by a distance of 1.27 cm (1/2 inch) so that  $r/a$  is equal to 1. A current density  $10^8$  A/m<sup>2</sup> and a wire cross-sectional area of 0.25 cm<sup>2</sup> ( $3.9 \times 10^{-2}$  in<sup>2</sup>) is assumed for both coils. Under these conditions the coils produce an interaction force on each other of approximately  $8 \times 10^{-7} \times (10^8)^2 \times (2.5 \times 10^{-5})^2 = 5$  N (1.1 lb). This is over a factor of 5 increase in comparable calculations for the distributed coil interaction case. Because both the distributed and the local coil interaction actuator designs can be used in the MAST

structure, these will be compared in further detail in the next major section of this report.

#### Use of Magnetostrictive Material

SatCon has expanded the focus of this research program to include an actuator approach which uses a new magnetostrictive material, Terfenol-D. This approach shows much potential as an actuator for intelligent structures. While the other approaches are based on magnetic forces which arise due to the interaction of currents, this approach is based on the property of magnetostrictivity. This means the material will produce strains under the influence of a magnetic field. This actuator approach is now very promising because the new material, Terfenol-D, has shown much stronger magnetostrictive properties than other materials. Furthermore, it has a factor of 10 improvement in both strain capability and energy density of piezoelectric materials. SatCon has included some preliminary results in this report. Further analysis is proposed under an initial task in Phase II, to compare the use of Terfenol-D with the other actuator approaches in this program. Phase II will then identify one concept to develop into a baseline prototype lab model.

#### Magnetostriction

Useful magnetostrictive materials produce large strains (extensions) when subjected to magnetic fields. In most materials this effect is quite small. For example, magnetostrictive strains in Nickel are on the order of 10 parts

per million (microstrain). The rare earth elements, however, possess a number of extraordinary magnetic properties. One of these properties is the ability to produce large magnetostrictive strains. During the 1960's and early 70's a variety of rare earth materials with large magnetostrictive strains, on the order of 1% (10,000 microstrain) were found. These materials, however, only exhibited these large magnetostrictive strains at low temperatures.

During the 1970's, a variety of new rare earth compounds that exhibit high levels of magnetostriction at room temperature were developed. These rare earth/iron compounds have large magnetostrictive strains of up to 0.2% (2000 microstrain) and Curie temperatures of over 500 degrees Fahrenheit. Researchers at the Ames Laboratory of the Department of Energy and at the Naval Surface Weapons Center have further developed these compounds and their manufacturing processes to the point where they have recently become commercially available under the brand-name Terfenol-D. Terfenol-D is formed from the rare earths terbium and dysprosium and from iron ( $Tb_{0.3}Dy_{0.7}Fe_{1.93}$ ) which is directionally solidified by free-stand-zone-melt (FSZM) process to near single crystal or directionally solidified by the Modified Bridgman process. The resulting material is available in rods of up to 1.5 inches (3.8 cm) in diameter. This stock can then be sliced into lamination thicknesses if desired.

Because of these recent developments, large-strain magnetostrictive materials capable of room temperature operation

are now available as the engineering material Terfenol-D. The most important property of Terfenol-D is its magnetostrictive characteristics. Like all magnetostrictive materials, its strain ( $\epsilon$ ) is a function of both the stress ( $\sigma$ ) and the applied magnetizing field ( $H$ ) as

$$\epsilon = f(\sigma) + g(H) \quad (32)$$

This relation for Terfenol-D is shown in Figure 28. Shown are curves of strain (in parts per million or microstrain) versus applied magnetizing field (in Oersteds) for various levels of compressive stress. These curves are found placing a Terfenol-D

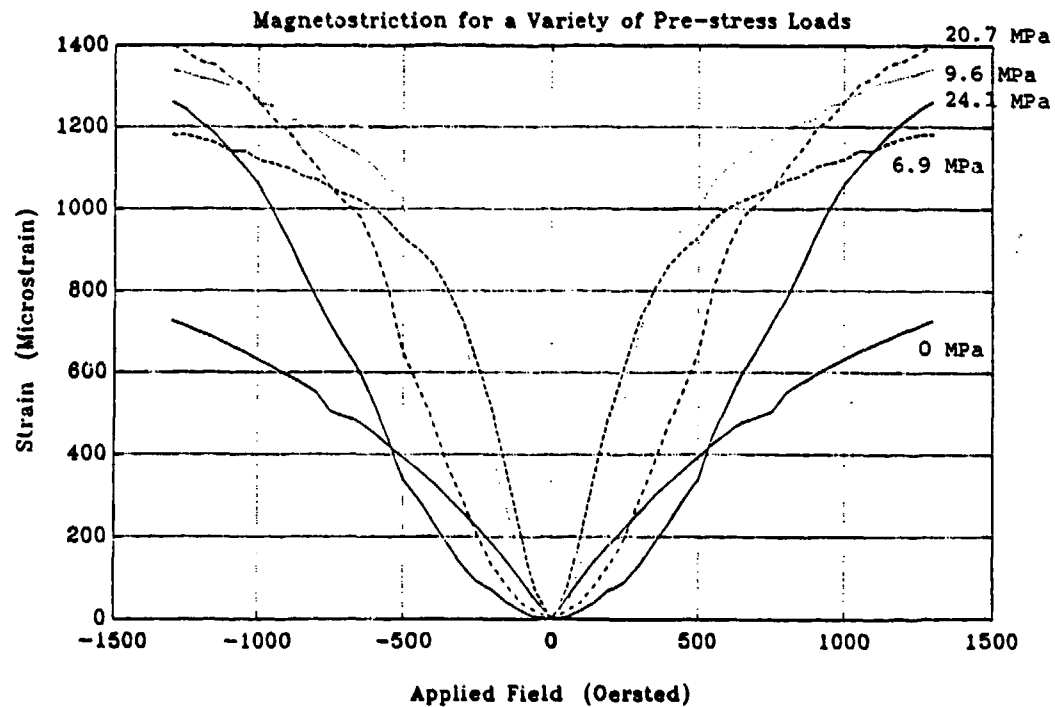


Figure 28 Magnetostriction of Terfenol-D vs Applied Magnetic Field

rod inside an electrical solenoid and axially compressing the Terfenol-D with a fixed load (fixed stress). The electric current in the solenoid is then varied, which varies the applied magnetizing field (H). The resulting axial expansion (tensile strain) of the Terfenol-D rod is then measured.

Many of the important characteristics of Terfenol-D can be seen in Figure 28<sup>23</sup>. The maximum strain is about 0.2% (2000 microstrain), approximately 10 times better than piezoelectric materials. The strain curves are symmetrical about the zero applied field point reflecting the fact that Terfenol-D contracts for both positive and negative magnetic field orientations. The magnetostrictive phenomenon is much stronger when the material is under compressive stress. The change in strain for unit change in applied field is strongest at applied fields of approximately 500 Oersted. Because of these properties, Terfenol-D is best utilized when it is preloaded with compressive stress and biased with a dc magnetic field.

The operation of Terfenol-D actuators can be explained with the simple subsystem shown in Figure 29. Shown is a Terfenol-D rod surrounded by an electric solenoid. A simple model of this subsystem would include the solenoid coil current and stress in the Terfenol-D as external inputs. The outputs are the strain in the Terfenol-D rod and the coil voltage. In addition to this Terfenol-D subsystem, a complete model of the actuator would include the stress-strain relation that the mechanical subsystem of the actuator would impose on the Terfenol-D.

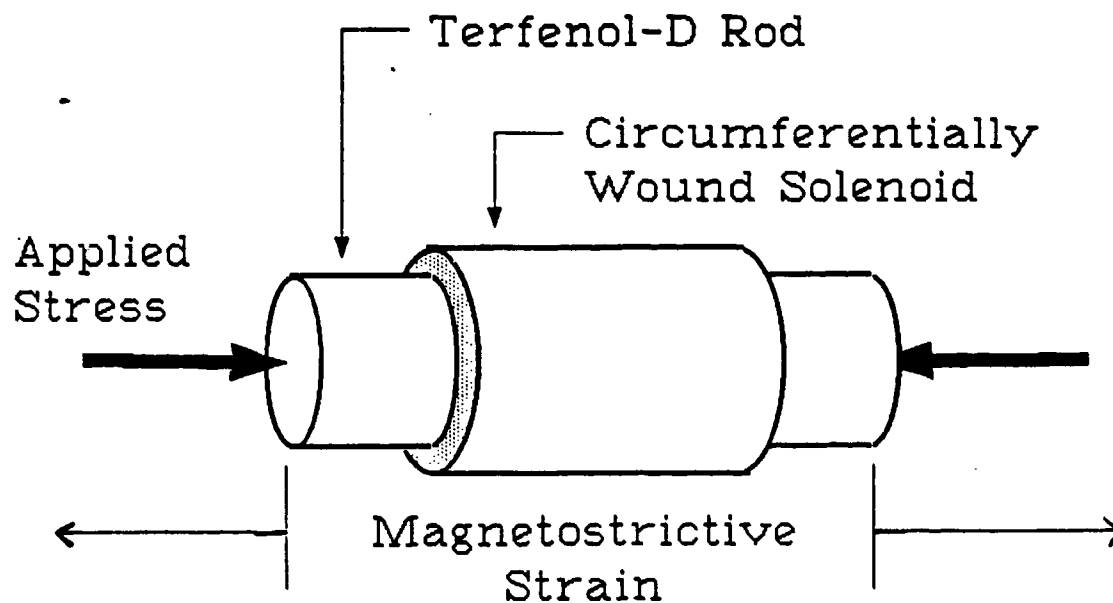
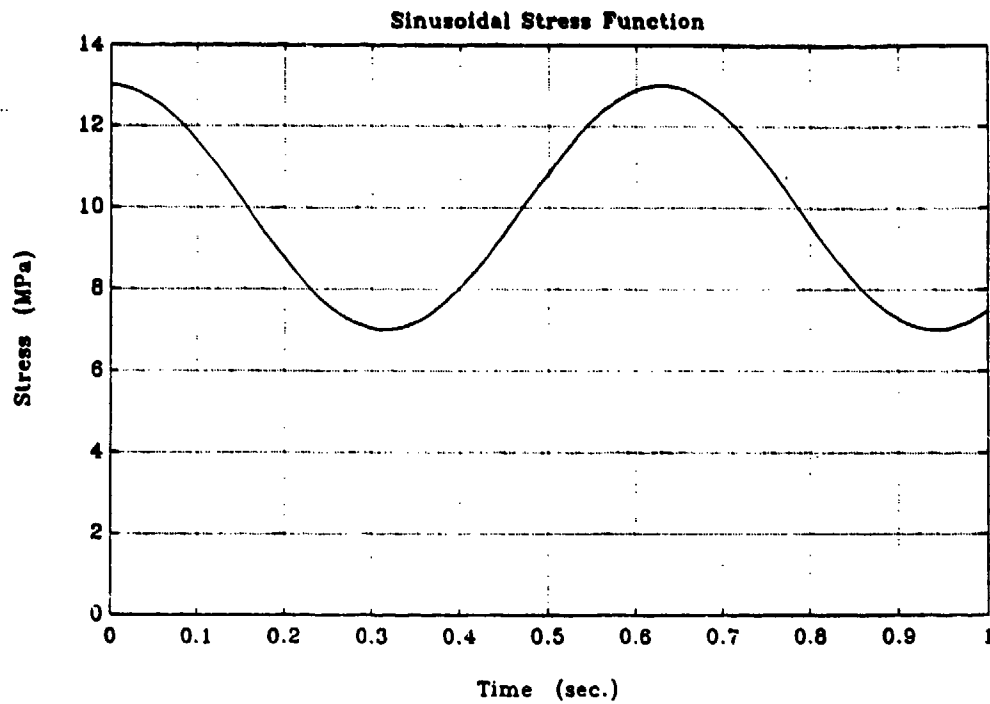
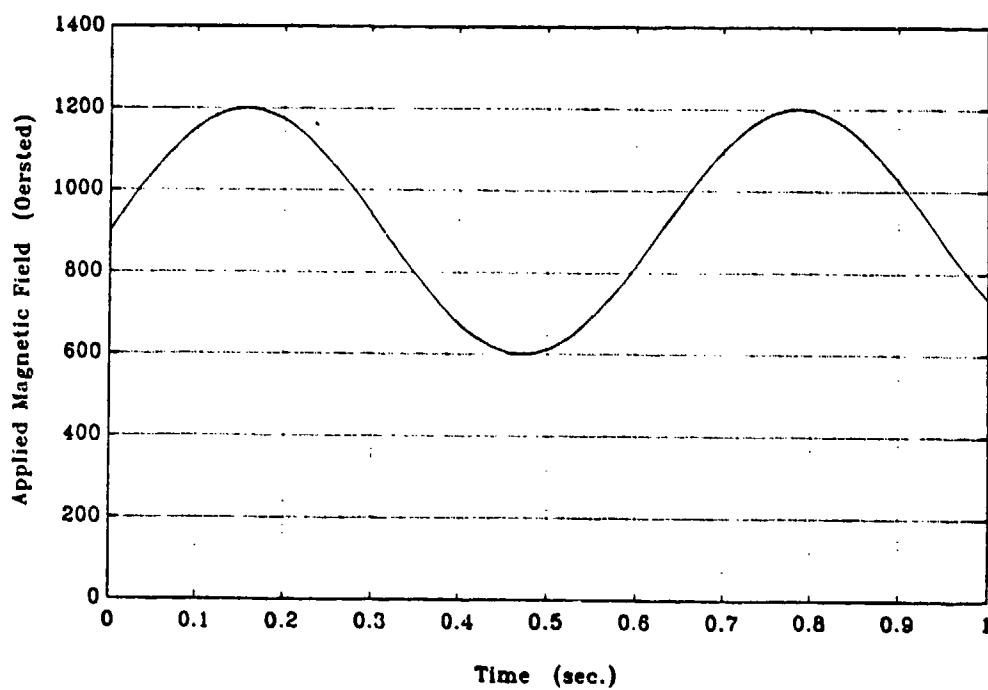


Figure 29 Simple Magnetostrictive Actuator

The mechanical power produced by the actuator can be found from the stress-strain curve over a cycle. For example, if the stress and applied field waveforms of Figures 30 and 31 are applied to the Terfenol-D, the resulting stress-strain relation shown in Figure 32 can be found using the curves of Figure 28. The area enclosed by the stress-strain loop of Figure 32 is simply the mechanical energy per unit volume that is produced by the Terfenol-D. This energy density can be as high as  $25\text{kJ/m}^3$  ( $0.67\text{ BTU/ft}^3$ ), approximately an order of magnitude higher than for piezoelectric materials.



**Figure 30 Example Stress Waveform in Terfenol-D**



**Figure 31 Example Applied Magnetic Field Waveform in Terfenol-D**

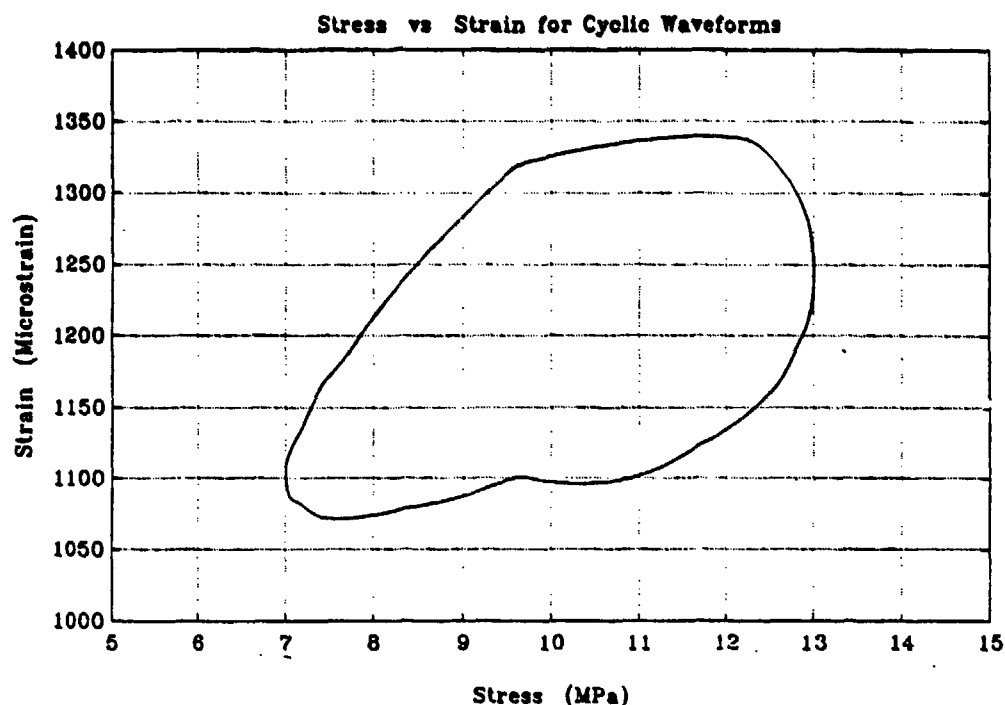


Figure 32 Stress vs Strain in the Terfenol-D for the Example Waveforms

The mechanical power output of the actuator depends both on the energy delivered during the cycle and the frequency of operation. If the actuator were run at 1000 Hz, power densities of up to 2.5 kW/kg (1.5 hp/lb<sub>m</sub>) are possible. Note that this is approximately 10 times the power density (approximately 0.1 hp/lb<sub>m</sub>) for conventional electric motors. Higher frequency operation resulting in higher power densities is also possible. The efficiency (mechanical output power/electrical input power) of the actuator can be 50% or greater. Losses are dominated by the magnetic hysteresis losses in the Terfenol-D, but also include resistive losses in the solenoid and eddy current losses, which can be minimized by the use of laminations, in the

## Terfenol-D.

Besides the stress/strain/magnetic field properties shown in Figure 28, other important properties of Terfenol-D are given in Table 3 below<sup>25</sup>. The high compressive strength of Terfenol-D combined with the greater magnetostriction when under compression means that Terfenol-D should nominally be under compression.

Table 3. Terfenol-D Properties

### Mechanical

|                      |                                   |  |
|----------------------|-----------------------------------|--|
| Density              | $9.25 \times 10^3 \text{ kg/m}^3$ | $0.33 \text{ lb}_m/\text{in}^3$          |
| Young's Modulus      | 25-35 GPa                         | $3.6\text{-}5.0 \times 10^6 \text{ psi}$ |
| Tensile Strength     | 28 MPa                            | 4.1 ksi                                  |
| Compressive Strength | 700 MPa                           | 100 ksi                                  |

### Thermal

|                   |                                       |
|-------------------|---------------------------------------|
| Thermal Expansion | $12 \times 10^{-6} \text{ /degree C}$ |
|-------------------|---------------------------------------|

### Magnetic

|                            |            |
|----------------------------|------------|
| Relative Permeability      | 4 - 6      |
| Mechanical Coupling Factor | 0.7 - 0.75 |

In summary, Terfenol-D is an exciting new material that will allow the design of novel electromagnetic actuators. It is particularly well suited to applications, such as distributed actuators, that require a combination of large forces, relatively small motions, high bandwidth, and good transient response. Compared to piezoelectric materials, it offers a factor of ten improvement in strain, energy density, and power density without requiring the high voltages typical of piezoelectric actuators.

Properly designed, Terfenol-D based actuators can have power densities an order of magnitude greater than conventional electric motors and solenoids. In addition Terfenol-D based actuators can be simply controlled.

This brief investigation into the properties of Terfenol-D show that exciting new actuator designs can be developed based on its unique properties.

#### **Summary of Actuator Design Section**

In this section, magnetic analyses were reviewed briefly in order to present the actuator design types considered. Five actuator designs were considered: interaction of distributed coils with the Earth's magnetic field, interaction of distributed coils with a large flux source, interaction of distributed coils with each other, local interaction of coils on a flexible structure truss element, and use of a magnetostrictive material, Terfenol-D. The first two approaches were shown to be undesirable for control of the beam model used in this investigation. Further comparative analysis of the distributed coil interaction approach and the local interaction approach is presented in the next section. The use of Terfenol-D is very promising and requires a more complete analysis. This analysis is being proposed as an initial task for Phase II.

#### **COMPARISON OF ACTUATOR APPROACHES**

In this section further analysis is presented to compare the more promising actuator approaches, ie the distributed coil

interaction and the local coil interaction. The actuator approach requiring the use of Terfenol-D, which is very promising, requires further analysis in Phase II. The local and distributed actuator approaches were compared in two ways. The first comparison was a mass and power comparison and was calculated by matching actuator force. The second comparison was done on the basis of energy removed from the baseline flexible structure model developed under task 1. The second methodology quantifies both the concepts of control effectiveness and the optimum actuator location for control of a vibrating beam. The control effectiveness is a function of both actuator type and mode shape.

#### Force Comparison

One way to compare the local and distributed actuator schemes is to match the vertical force transmitted by the actuators to the beam and then to compare the required mass and power to obtain this force (For the local interaction scheme, the truss-beam interaction is modelled as if the beam imposed a kinematic constraint of no deflection, thus force and not deflection is transmitted to the beam.). For the local actuator approach, mass and power comparison calculations were performed using a current density of  $10^8 \text{ A/m}^2$  ( $9 \times 10^6 \text{ A/ft}^2$ ), wire cross-sectional area of  $1 \text{ cm}^2$  ( $0.155 \text{ in}^2$ ), and coil radius of  $1.27 \text{ cm}$  ( $1/2 \text{ inch}$ ). The ratio of separation distance ( $r$ ) to coil radius ( $a = 1.27 \text{ cm} = 1/2 \text{ in}$ ) is varied from 1 to 4. This is the near field range where Maxwell's mutual inductance formula (30) is

appropriate. These values are also appropriate for implementation in the MAST model. Aluminum conductor was assumed for both the local and the distributed actuator approaches. Parameters compatible with the MAST model were also chosen for the distributed case. In this case, coil separation distance ( $r$ ) was equal to the distance between the distributed coils if they were located at the ends of a MAST truss section. Because the MAST trusses were 1.6 m long (5.2 ft) with a truss angle of  $47^\circ$ , the separation distance for the coils is  $1.6\cos 47^\circ$  m ( $5.2\cos 47^\circ$  ft). The coil radius for the coils in the distributed case were chosen to be 5 cm (1.97 in). Notice that this value of  $r/a = 20$  is appropriate for the dipole far field equations (Equations (25) and (26)). Magnetic moments of the coils for the distributed case, were chosen to match the vertical force transmitted to the beam calculated in the local case. Figure 33 is a plot of mass vs vertical force transmitted to the beam. Figure 34 is a plot of power vs. vertical force transmitted to the beam. If the coils were superconducting, no power would be required. The plots show that the local interaction scheme requires both less mass and less power than the distributed scheme. The larger forces are obtained for the cases where the coils are close together. Thus  $r/a=1$  is the point corresponding to the largest force of approximately 0.4 N (0.09 lb) in Figures 33 and 34. This comparison is useful as it gives the tradeoff between mass, power, and force.

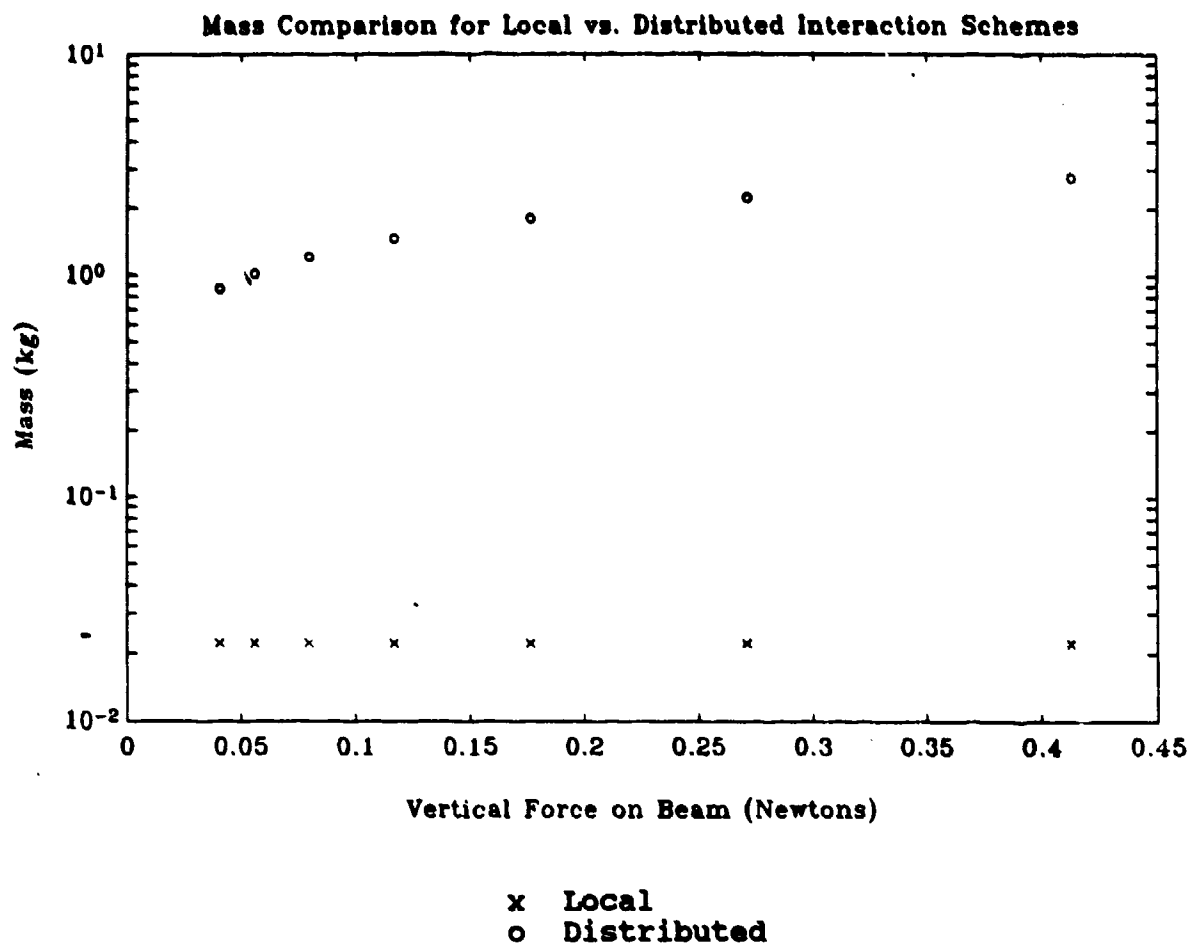


**Figure 33 Mass Comparison of Local vs Distributed Actuator Concepts**

#### **Control Effectiveness and Optimum Actuator Location Derivation of Control Effectiveness**

A methodology is developed in this section to determine the optimum location for removing power from a vibrating beam using the local or distributed actuators. The local and the distributed coil interaction schemes are then compared using this methodology. The approach is to consider the energy removed from the beam as a function of actuator force and/or torque and modal displacements, and then maximize the energy removed with respect to the modal parameters.

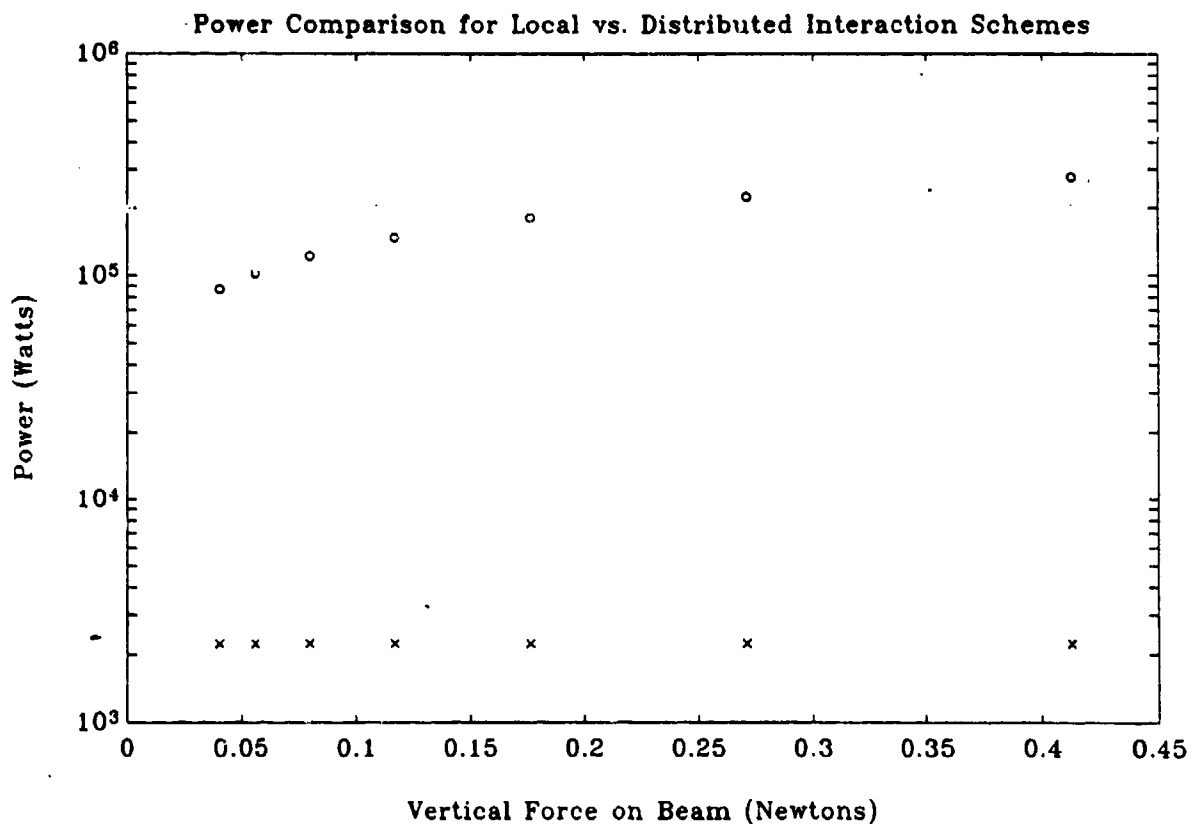


Figure 34 Power Comparison of Local vs Distributed Actuator Concepts

For example, an actuator which produces a single force would remove power from the beam as follows:

$$P = F \cdot y \cdot \omega \quad (32)$$

where

$F$  = Actuator Force

$y$  = Translational Displacement at Actuator Location

$\omega$  = Modal Frequency

Therefore the energy removed per cycle is given by:

$$E = F \cdot y \quad (33)$$

On the other hand, an actuator which produces a single torque would remove power from the beam given by the following expression.

$$P = r \cdot \theta \cdot \omega \quad (34)$$

where

$r$  = Actuator Torque

$\theta$  = Rotational Displacement at Actuator Location

$\omega$  = Modal Frequency

Energy removed per cycle by a single torque actuator is therefore:

$$E = r \cdot \theta \quad (35)$$

The actuators considered here are not single force or torque actuators. They produce both force and torque. A general expression can be written for the energy removed per cycle from a beam:

$$E = \sum_{i=1}^n F_i y_i + \sum_{j=1}^m r_j \theta_j \quad (36)$$

where there are  $n$  actuator forces and  $m$  actuator torques. This is obtained by summing the energy removed per cycle at each actuator location. This term will be referred to in this paper as the control effectiveness of the actuators. Later comparisons of the

ability of the different actuator types in damping out the vibrations of a beam will be made using this concept.

If a sinusoidal mode shape is assumed, the translational displacement ( $y$ ) for the beam can be written as:

$$y = A \sin \left( \frac{2 \pi x}{l} \right) \quad (37)$$

where  $x$  is the axial position and  $l$  is the beam length.

Using Bernoulli-Euler beam theory the rotational displacement,  $\theta$ , is obtained by taking the derivative with respect to  $x$ .

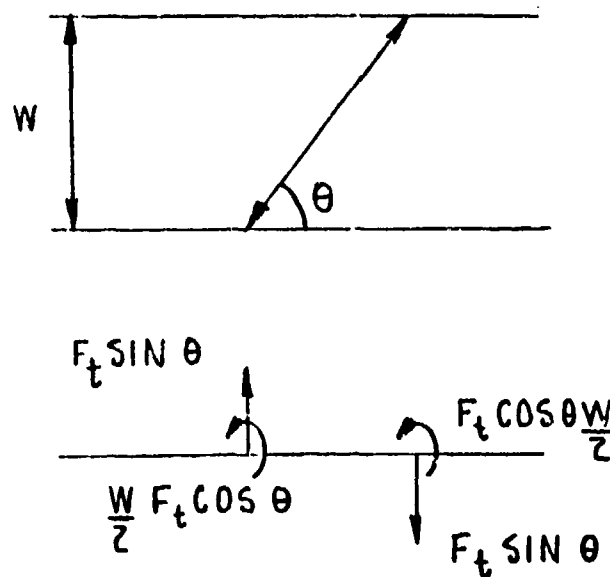
$$\theta = \left( \frac{2 \pi}{l} \right) \cos \left( \frac{2 \pi x}{l} \right) \quad (38)$$

#### Comparison of Control Effectiveness for Distributed and Local Cases

Expressions for the energy removed per cycle (effectiveness) will be derived for the distributed coil interaction case and several variations of the local coil interaction case.

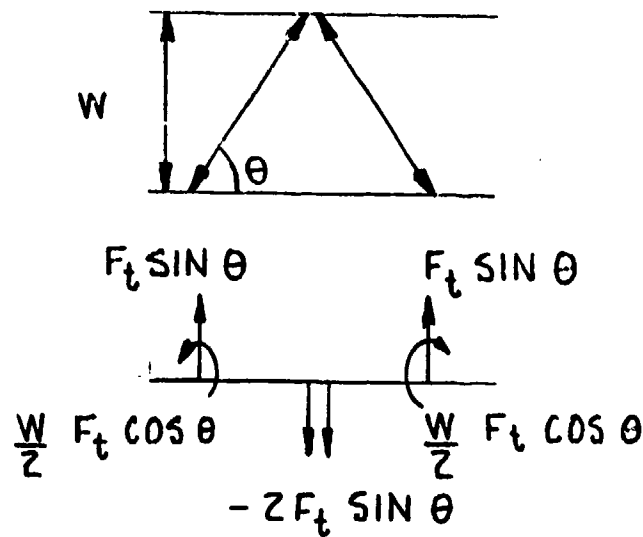
The truss beam-interaction for the local case is modelled as if the beam imposes a kinematic constraint of no beam deflection. This type of model was shown in Figure 27(a) where the force transmitted from the truss to the beam is shown to be proportional to the ratio of coil separation distance to truss length. There are three variations of the local actuator approach that are considered. The first is a one truss actuator that is in tension (or compression). The second is a two truss actuator in which both trusses are simultaneously either in tension or in compression. The third approach is a two truss

actuator in which one truss is in tension and the other truss is in compression. These variations on the local actuator approach and associated force modelling assumptions are shown in Figure 35. Notice from these figures that axial effects on the beam are neglected because only beam bending is being modelled. These models are appropriate for use in conjunction with the finite element beam model developed previously. The elements are point nodes; hence, the model of the beam-truss interaction is one which uses an equivalent force system on a node located on the neutral axis of the beam. Notice in Figure 35 the notation " $F_t$ " denotes the force transmitted to the beam by the truss, " $\theta$ " is the truss angle, and " $w$ " is the beam width. The one truss actuator produces a moment and a force on nodes which correspond

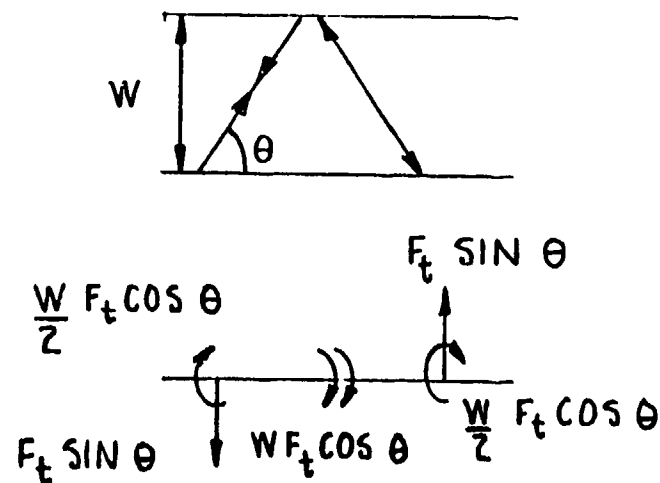


(a) One Truss Actuator

Figure 35 Modelling Assumptions Appropriate for Use in Finite Element Beam Model for Local Interaction Actuator Schemes (continued on next page)



- (b) Two Truss Actuator in which Both Trusses are Simultaneously Either in Tension or in Compression



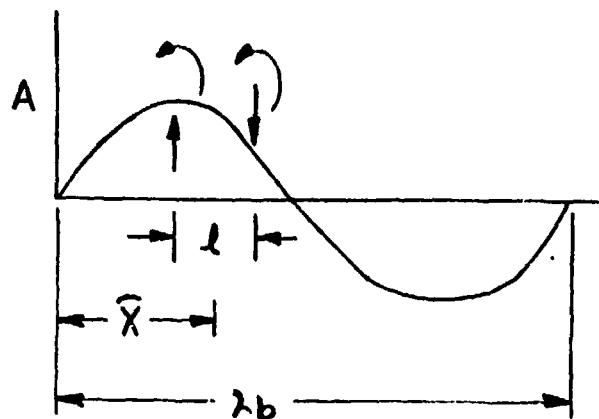
- (c) Two Truss Actuator in which One Truss is in Tension and the other is in Compression

Figure 35 Modelling Assumptions Appropriate for Use in Element Beam Model for Local Interaction Actuation Schemes

to the axial location of the ends of the truss Figure 35(a). The force and torque on the structure produced by this actuator, as well as the other types of actuators, is zero, as expected from Newton's Action-Reaction Law. The two truss actuators can be modelled by force and torque effects at three nodes. For the two truss actuator that has both trusses in either tension or compression (Figure 35(b)), the two outer nodes undergo forces of the same direction and magnitude and torques of opposite directions and the same magnitude. The middle node, which corresponds to the truss intersection location, undergoes a force that is twice the magnitude of one of the individual forces on an outer node. Again, by adding up these forces and torques, the net effect is zero. The third actuator approach (two truss compression-tension) produces a different effect on the overall beam structure (Figure 35(c)). The middle node has a moment that is twice as strong and in the opposite direction as the moments on the outer nodes. The outer nodes have forces which are equal in strength but opposite in direction.

The distributed actuator approach can be modelled in a similar way (Figure 19). This model has two nodes located at the positions of the two coils. The two forces produced are of equal magnitude and opposite direction. The two torques produced in the coils cancel the net moment produced by the forces.

Because the distributed case and the one truss local case reduce to similar force effects on the beam, a common terminology is introduced (Figure 36). The mean location of the actuator



|                 |  |
|-----------------|--|
|                 | $\alpha = 2 \pi \frac{\bar{X}}{\lambda_b}$ |
| Mean Location   |  |
|                 | $\beta = \pi \frac{l}{\lambda_b}$          |
| Coil Separation |  |

Figure 36 Definition of Mean Location,  $\alpha$ , and Coil Separation,  $\beta$ , for Sinusoidal Mode Shape

force and torque application points normalized by the wavelength of mode,  $\lambda_b$ , is denoted by  $\alpha$ :

$$\alpha = \frac{2 \pi \bar{X}}{\lambda_b} \quad (39)$$

where  $\bar{X}$  is the distance of along the length of the beam of the mean location of the force and torque application points. The term  $\beta$  denotes the coil separation; again this term is normalized

by the wavelength of the mode.

$$\beta = \frac{\pi l}{\lambda_b}$$

where  $l$  is the distance between force application points. Expressions for the control effectiveness  $E$  (energy removed per unit cycle) were derived using Equation (36) for each actuator type being compared. These expressions are shown in Table 4.

Table 4 Effectiveness Expressions for Local and Distributed Actuator Types

|   | <u>Effectiveness Expression</u>   |
|---|---|
| Local One Truss                         | $2FA \cos \alpha [\beta \cos \beta - \sin \beta]$   |
| Local Two Truss<br>Tension-Tension      | $4FA \sin \alpha [\sin^2 \beta - \frac{\beta}{2} \sin (2\beta)]$<br><br>$\text{small } \beta \quad E \propto \beta^4$ |
| Local Two Truss<br>Compression-Tension  | $2AF \cos \alpha [\sin (2\beta) - 2\beta \cos^2 \beta]$<br>$\text{small } \beta \quad E \propto \beta^3$              |
| Distributed "Configuration<br>2" Scheme | $2FA \cos \alpha \sin \beta - 2\beta FA \cos \alpha \cos \beta$<br>$+ \frac{2}{3} \beta FA \sin \alpha \sin \beta$    |

In these expressions, "A" is the amplitude of vibration and "F" is the vertical force transmitted to the beam. Effectiveness was calculated in order to determine which local actuation scheme is the most useful for flexible structure control of the MAST beam model. The calculations were performed for one actuator located at its optimum location on the flexible beam model

developed previously. The optimum location is found by maximizing the effectiveness term with respect to the mean location " $\alpha$ ". The results of these calculations are shown in Figures 37 and 38. Figure 38 is plotted on a logarithmic scale to emphasize what happens when  $\beta$  is small. This is of interest because the flexible structures have low natural frequencies, long wavelengths and thus small  $\beta$ 's. Using Figure 38, the local

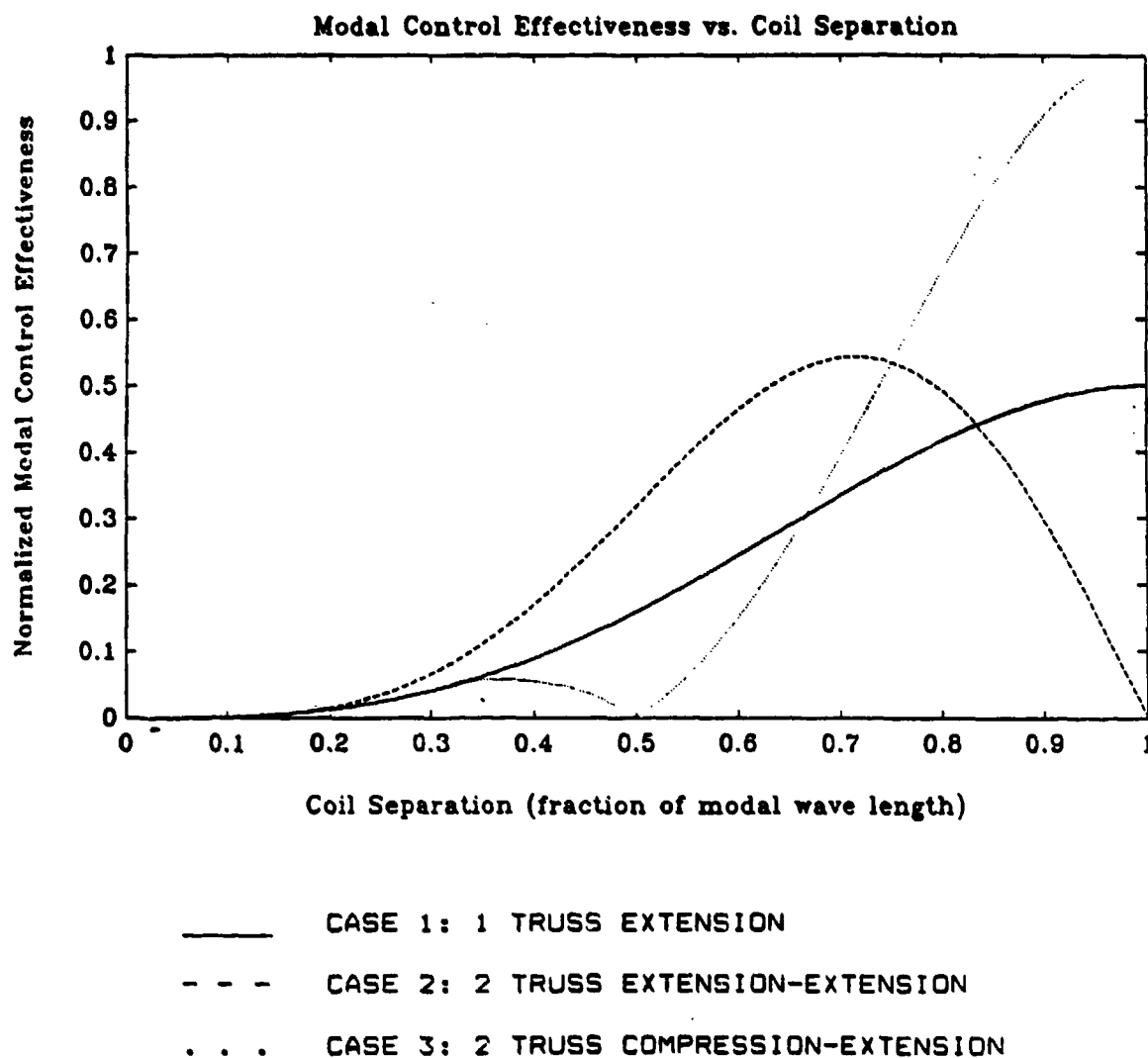
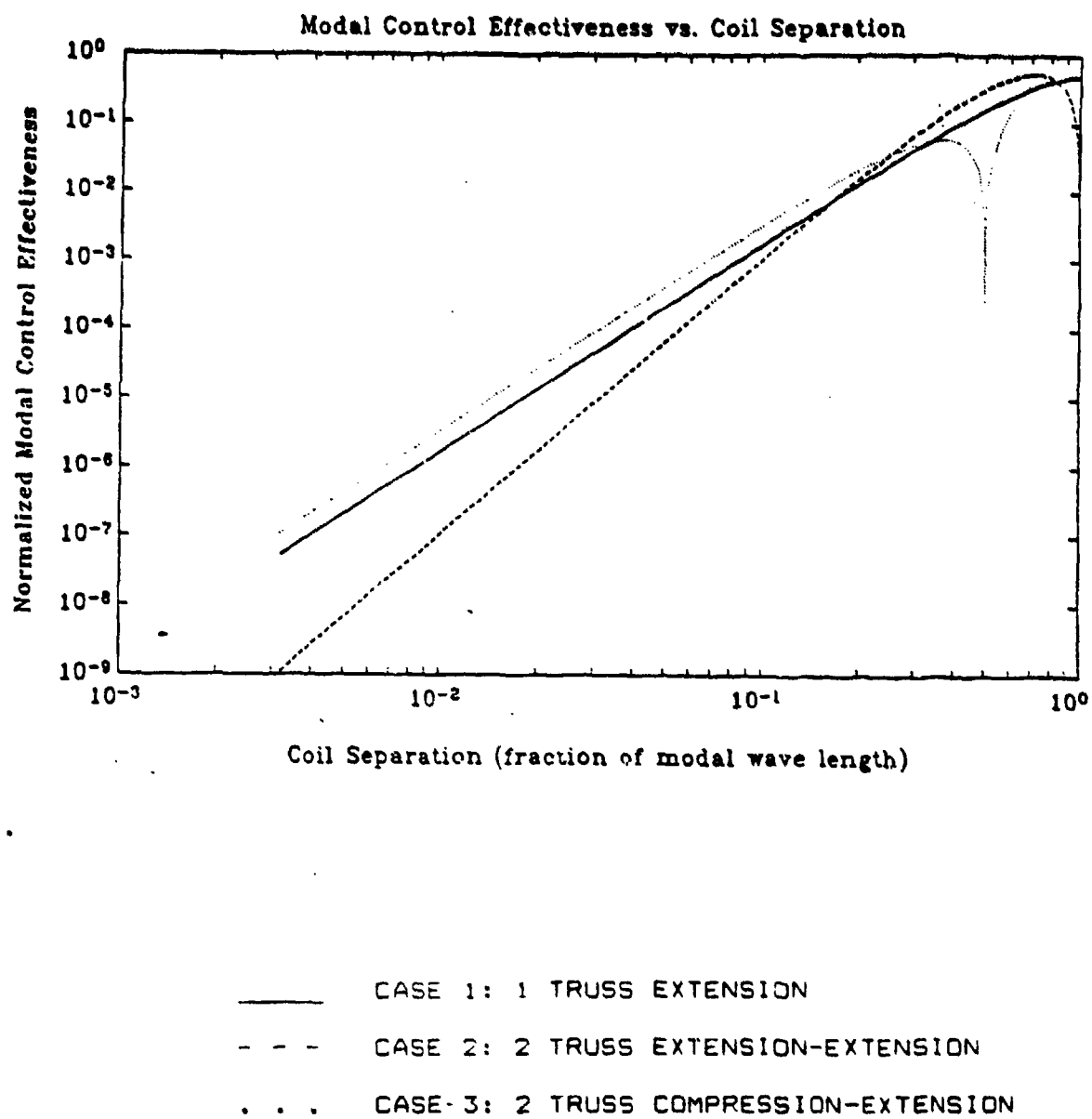


Figure 37 Control Effectiveness vs Coil Separation



**Figure 38 Control Effectiveness vs Coil Separation**

interaction variations can be compared. This plot shows that an actuator consisting of two trusses, one undergoing compression and the other undergoing extension, is more effective for small  $\beta$ 's than a one truss extension or a two truss extension-extension. In fact, it can be shown, using Taylor series expansions, that the effectiveness for the truss extension-compression case is proportional to  $\beta^3$  while the effectiveness for the truss extension-extension case is proportional to  $\beta^4$ .

Table 5 is a summary of effectiveness calculations on a per mass and per power basis for the distributed interaction scheme and two variations on the local one truss interaction scheme. Because the MAST deployable beam structure has truss angles of  $47^\circ$  for some of its structural trusses, one local scheme considered in these comparisons also uses a truss angle of  $47^\circ$ . Analysis, however, showed that for the purpose of removing energy from a vibrating beam with the actuators considered, a truss angle of  $30^\circ$  is more effective. Thus a second local scheme is considered with a truss angle of  $30^\circ$ . The modal wavelength used in these calculations is 60 m (197 ft), which is the length of the MAST structure, and a non-superconducting current density level of  $10^6$  A/m<sup>2</sup> ( $9 \times 10^4$  A/ft<sup>2</sup>) is assumed. The chart shows that these local interaction schemes are two orders of magnitude better than the distributed interaction scheme on both an effectiveness per mass and an effectiveness per power basis. The best effectiveness per mass per vibration amplitude (energy removed per cycle from a vibrating beam per kg of actuator mass

Table 5 Effectiveness Calculations

Modal Wavelength: 60 m

Current Density:  $10^6$  A/m<sup>2</sup>

|  | $\frac{E}{A}$          | $\frac{J}{m \text{ cycle}}$ | $\frac{E}{Am}$         | $\frac{J}{mKg \text{ cycle}}$ | $\frac{E}{AP}$        | $\frac{J}{m \text{ Watt cycle}}$ |
|--|------------------------|-----------------------------|------------------------|-------------------------------|-----------------------|----------------------------------|
| Distributed Interaction<br>"Standard" Size<br>Dipoles 10 m Apart   | $7.78 \times 10^{-10}$ |                             | $2.38 \times 10^{-10}$ |                               | $2.6 \times 10^{-11}$ |                                  |
| One Truss Local Interaction Scheme<br>for MAST<br>Truss Angle $47^\circ$<br>Truss Length 1.6 m<br>Wire C.S. Area $(1/2)^2 \text{ cm}^2$<br>Coil Radius 1.27 cm | $3.2 \times 10^{-10}$  |                             | $2.9 \times 10^{-8}$   |                               | $2.9 \times 10^{-9}$  |                                  |
| One Truss Local Interaction Scheme<br>Truss Angle $30^\circ$<br>Truss Length 1.6 m<br>Wire C.S. Area $(1/2)^2 \text{ cm}^2$<br>Coil Radius 1.27 cm             | $4.5 \times 10^{-10}$  |                             | $4.1 \times 10^{-8}$   |                               | $4.1 \times 10^{-9}$  |                                  |

per vibration amplitude) in this chart is  $4 \times 10^{-8}$  J/m kg cycle ( $5 \times 10^{-12}$  Btu/ft lbm cycle) and  $4 \times 10^{-9}$  J/m watt cycle ( $8.6 \times 10^{-10}$  Btu/ft hp cycle) for the local two  $30^\circ$  truss extension-compression case.

Because of the simplifying modelling assumptions used in this Phase I investigation, these effectiveness numbers should only be used for comparing the different actuator approaches. In particular, these calculations are based on extreme models of truss-beam interactions. In either extreme model discussed

earlier (zero force vs zero deflection Figure 27), the desired effect (force or deflection) is reduced by a factor of  $r/l$  (separation distance to truss length) if the coils are placed in the middle of the truss. If two sets of coils are placed close to the ends of the truss, however, an equivalent simple model will increase by a factor of  $l/r$  the effectiveness calculated using the rigid beam model.

The coils are capable of producing adequate forces. As shown earlier, with current densities of  $10^8 \text{ A/m}^2$  ( $9 \times 10^6 \text{ A/ft}^2$ ), the local interaction case was shown to be capable of 5 N (1.1 lb) for geometrical parameters appropriate for MAST. Because of the simplifying modelling effects, further effectiveness analysis is suggested as an initial task in Phase II.

Tables 6 and 7 are similar charts which show the same effect for different wavelengths and/or current densities. The trend showing the local interaction is better than the distributed interaction in an effectiveness per mass basis is again shown in these charts. Table 6 is for a wavelength of 360 m (1181 ft), and a non-superconducting current density. By comparing this chart with the previous chart (Table 5) it can be seen that the effectiveness decreases with increasing wavelength. This is to be expected as the equations for effectiveness for small  $\beta$  (Table 4) show that the effectiveness is proportional to a power of  $\beta$  and thus inversely proportional to wavelength.

Table 6 Effectiveness Calculations

Modal Wavelength: 360 m

Current Density:  $10^6$  A/m<sup>2</sup>

|   | $\frac{E}{A}$         | $\frac{J}{m \text{ cycle}}$ | $\frac{E}{Am}$        | $\frac{J}{mKg \text{ cycle}}$ | $\frac{E}{AP}$        | $\frac{J}{m \text{ Watt cycle}}$ |
|---|-----------------------|-----------------------------|-----------------------|-------------------------------|-----------------------|----------------------------------|
| Distributed Interaction<br>"Standard" Size<br>Dipoles 10 m Apart  | $2.0 \times 10^{-11}$ |                             | $6.1 \times 10^{-12}$ |                               | $6.1 \times 10^{-13}$ |                                  |
| One Truss Local Interaction Scheme<br>for MAST<br>Truss Angle $47^\circ$<br>Truss Length 1.6 m<br>Wire C.S. Area $(1/2)^2 \text{cm}^2$<br>Coil Radius 1.27 cm | $1.5 \times 10^{-12}$ |                             | $1.3 \times 10^{-10}$ |                               | $1.3 \times 10^{-11}$ |                                  |
| One Truss Local Interaction Scheme<br>Truss Angle $30^\circ$<br>Truss Length 1.6 m<br>Wire C.S. Area $(1/2)^2 \text{cm}^2$<br>Coil Radius 1.27 cm             | $2.1 \times 10^{-12}$ |                             | $1.9 \times 10^{-10}$ |                               | $1.8 \times 10^{-11}$ |                                  |

Table 7 is effectiveness calculations using a superconducting current density wavelength of 360 m (1181 ft), respectively. The effectiveness per power basis is not shown here because superconductors use no power. These numbers are an improvement by 4 orders of magnitude over their respective effectivenesses in Tables 6. The actuator type with the highest effectiveness can remove  $1.9 \times 10^{-6}$  J/m kg cycle ( $2.5 \times 10^{-10}$  Btu/ft lbm cycle).

Table 7 Effectiveness Calculations

Modal Wavelength: 360 m

Current Density:  $10^8$  A/m<sup>2</sup>

|   | $\frac{E}{A}$ | $\frac{J}{m \text{ cycle}}$ | $\frac{E}{Am}$ | $\frac{J}{mKg \text{ cycle}}$ |
|---|---------------|-----------------------------|----------------|-------------------------------|
| Distributed   |               | $2.0 \times 10^{-7}$        |                | $6.3 \times 10^{-8}$          |
| Interaction<br>"Standard" Size<br>Dipoles 10 m Apart  |               |                             |                |                               |
| One Truss Local<br>Interaction Scheme<br>for MAST<br>Truss Angle 47°<br>Truss Length 1.6 m<br>Wire C.S. Area $(1/2)^2 \text{cm}^2$<br>Coil Radius 1.27 cm |               | $1.5 \times 10^{-8}$        |                | $1.3 \times 10^{-6}$          |
| One Truss Local<br>Interaction Scheme<br>Truss Angle 30°<br>Truss Length 1.6 m<br>Wire C.S. Area $(1/2)^2 \text{cm}^2$<br>Coil Radius 1.27 cm             |               | $2.1 \times 10^{-8}$        |                | $1.9 \times 10^{-6}$          |

#### Summary of Actuator Comparison Section

In this section two types of actuator designs were compared: the local coil interaction and distributed coil interaction cases. Comparisons were performed on both a force and an energy basis. The local coil interaction was shown to be a better approach on a per mass and a per power basis for controlling beam vibrations. In addition, several variations on the local coil interaction scheme were examined.

## CONTROLLER DESIGN

The purpose of this section is to verify the open loop analysis developed previously for the effectiveness comparison of the various actuator schemes. This will be done by simulating the MAST model with approximately 200 local actuators of five Newton force (1.1 lb) capability actuators placed optimally on the structure. As stated earlier, the effectiveness numbers are strongly dependent on the modelling assumptions of the truss-beam interactions and should only be used to compare the different actuator approaches.

The method used to verify the open loop predictions is to plot time simulations of a vibrating beam placed under optimal control action using two different local actuation schemes. The time simulations should show that the scheme with the higher effectiveness will be able to damp the vibrations faster.

Two local interaction schemes are shown along with a diagram of the forces and moments which are transmitted to the beam. Each local interaction scheme consists of two truss structures. These are shown in Figures 35(b) and 35(c). Each truss has a pair of coils centered in the truss section. In the first local interaction scheme the coil forces are set up to produce tension in both trusses or compression in both trusses. The second local interaction scheme is set up to produce compression in one truss and tension in the other truss. Time simulations were performed with a mode 3 initial condition and a maximum transverse displacement of 1 cm (0.4 in). This mode has a

wavelength that is approximately the length of the beam (60 m (197 ft)) and a frequency of 5.7 Hz. The maximum transverse displacement occurs at the 20 m (65 ft) node. The mode shape is shown in Figure 5. Time simulations of the controlled structure are shown in Figures 39 and 40. The maximum vertical force transmitted to the beam was matched for both cases to be around 1000 N (225 lb). The effectiveness calculations presented previously predict that the compression extension scheme will remove more energy per unit time from a vibration beam than the extension-extension case. The time simulations verify this prediction. They show higher damping levels for the compression extension scheme.

#### CONCLUSIONS

This Phase I SBIR research has investigated the feasibility of using an array of magnetic coils for use as an actuation system for flexible structure control. Five actuator designs were compared. The first actuator design involved magnetic coils distributed in a flexible structure. These coils would produce control torques on the beam by interacting with the Earth's magnetic field. The second actuator design was control torque production by the interaction of distributed magnetic coils with a large flux source located on the spacecraft. The third actuator design produced control forces and torques by interacting distributed coils on the structure. The fourth was to place the coils very close together to obtain stronger forces

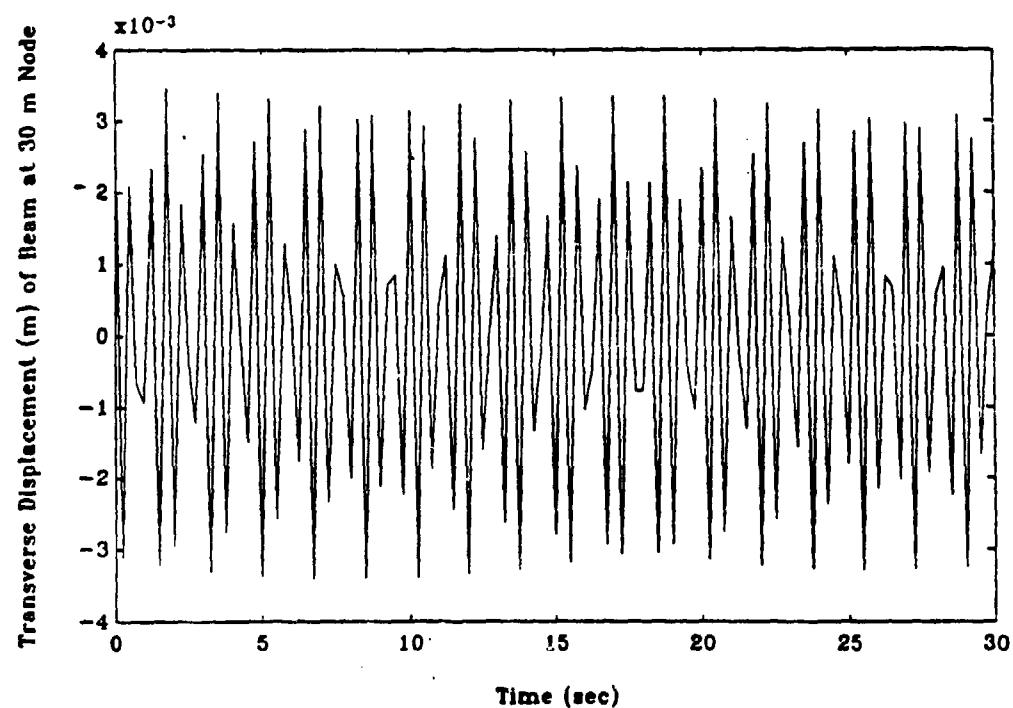
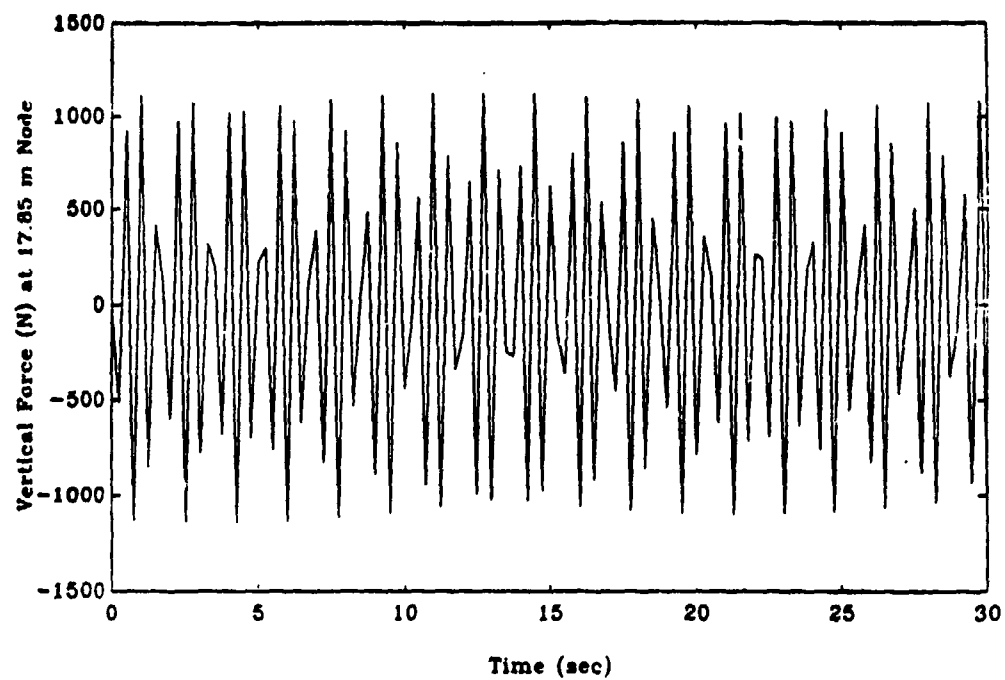


Figure 39 Time Simulations for Controlled Beam Using Two Truss Tension-Tension Local Interaction Scheme

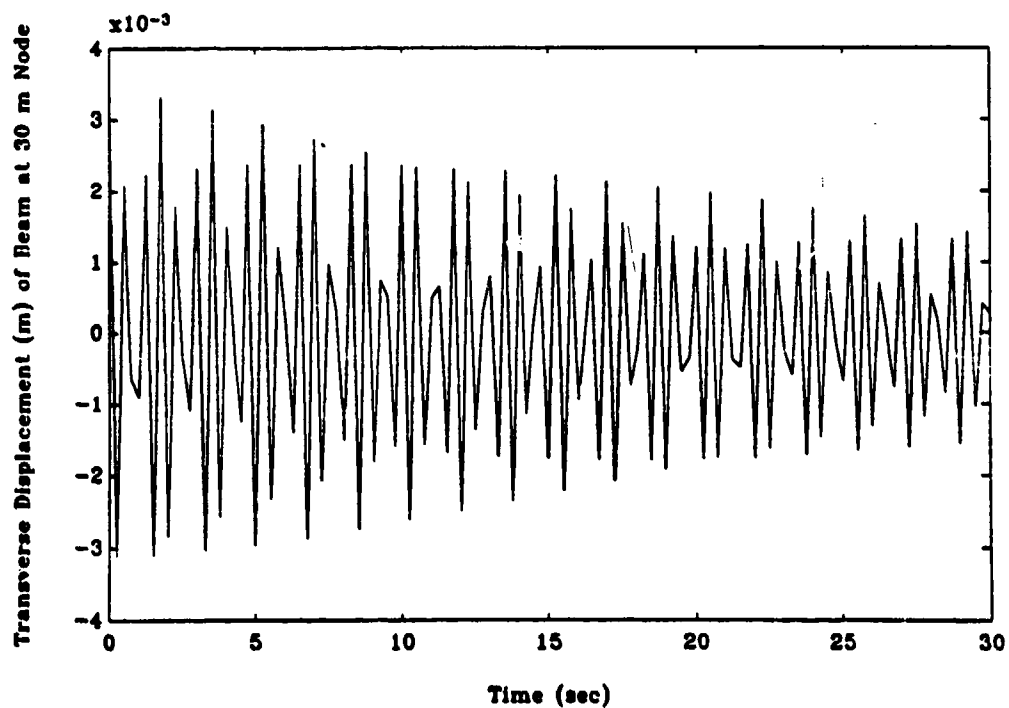
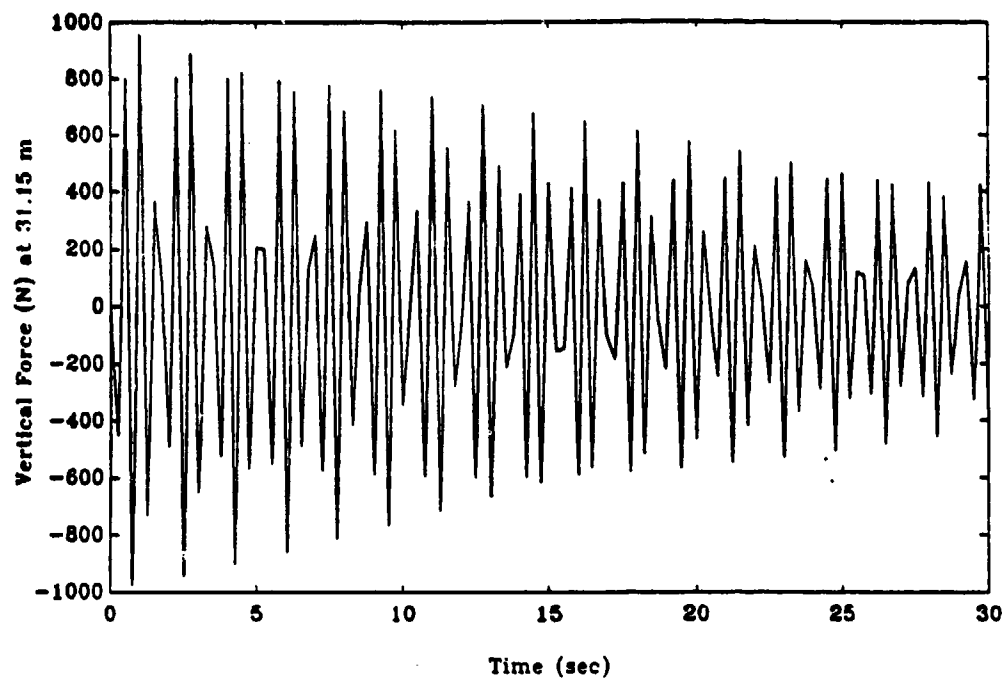


Figure 40 Time Simulations for Controlled Beam Using Two Truss Tension-Compression Local Interaction Scheme

and torques on the flexible structure. This approach was termed local interaction. The final actuator approach requires the use of a new material, Terfenol-D, which is magnetostictive, i.e., it strains under the presence of a magnetic field.

Initial investigations on each of these methods were performed. The interaction of distributed coils with the Earth's magnetic field would require the shape and vibration control system to depend strongly on the position of the actuator with respect to inertial space. Also, this method can only produce control torques because the force depends on the gradient of the magnetic field which is small for the distances associated with the magnetic coils. The second method, interaction with a large flux source, is only capable of torque production about two axes. And furthermore, there would be a torque on the large flux source which is large enough to interfere with attitude control. These first two actuator methods are undesirable for a MAST type structure. They may have application, however, to a spacecraft with combined rigid body attitude control and flexible structure control. The actuator approach using a new magnetostrictive material, Terfenol-D, was shown to be a very promising approach that requires further Phase II investigation.

The emphasis of this Phase I research was comparing the distributed coil and the local coil interaction methods. The local interaction approach transmits more force to the structure on both a per mass and a per power basis than does the distributed coil approach. A concept was developed which

quantifies the effectiveness of an actuator being used to damp vibrations in the MAST beam model. This concept is based on the amount of energy removed per cycle. Several variations of the local interaction actuator concept were then investigated. These included a one truss local actuator and two truss actuators. One type of two truss actuator had tension (or compression) in both trusses. The other type had tension in one of the trusses and compression in the other truss.

The open-loop effectiveness comparisons were verified by simulation. A controller was designed for the system using linear-quadratic methods. The two truss tension-tension case and the two truss compression-tension case were compared and verified the control effectiveness analysis.

Further comparative analysis of the local interaction approach and the Terfenol-D approach is recommended for Phase II research. Simpler analytical models, for example those that model strictly the actuator and truss section, are recommended. Phase II will include the design and construction of both types of prototype actuators. The use of the truss and actuator models will also allow comparison with more conventional actuator approaches such as piezoelectrics.

## REFERENCES

1. Nurre, G.S., Ryna, R.S., Scofield, H.N., and Sims, J.L., "Dynamics and Control of Large Space Structures", Journal of Guidance, Control and Dynamics, Volume 7, No. 5, pp. 514-526, September-October 1984.
2. Lenzi, D.C. and Shipley, J.W., "MAST Flight System Beam Structure and Beam Structural Performance", NASA/DoD Control/Structures Interaction Technology Conference, Norfolk, VA, 1986.
3. Ibid.
4. Brumfield, M.L., "MAST Flight System Operations", NASA/DoD Control/Structures Interaction Technology Conference, Norfolk, VA, 1986.
5. Ibid.
6. Bathe, K.J., Finite Element Procedures in Engineering Analysis, Prentice-Hall, Inc., Englewood Cliffs, NJ, 1982.
7. Ibid.
8. Ibid.
9. Ibid.
10. Ibid.
11. Ibid.
12. Ibid.
13. Lenzi, D.C. and Shipley, J.W., "MAST Flight System Beam Structure and Beam Structural Performance", NASA/DoD Control/Structures Interaction Technology Conference, Norfolk, VA, 1986.
14. Lorrain, P. and Corson, D.R., Electromagnetic Fields and Waves, W.H. Freeman and Company, San Francisco, CA, 1970.
15. Ibid.
16. Ibid.
17. Ibid.
18. Ibid.

19. Schwartz, M., Principles of Electrodynamics, McGraw Hill Book Company, New York, 1972.
20. Rosa, E.B. and Grover, F.W., "Formulas for the Calculation of Mutual and Self-Inductance", Bulletin of the Bureau of Standards, Department of Commerce and Labor, Vol. 8, 1912.
21. Handbook of Mathematical Functions with Formulas, Graphs, and Mathematical Tables, US Department of Commerce, National Bureau of Standards, No. 55, Washington, D.C., 1972.
22. Wertz, J.R., Spacecraft Attitude Determination and Control, D. Reidel Publishing Co., Boston, MA, 1985.
23. Clark, A.E. and Savage, H.T., "Magnetostriction of Rare Earth - Fe<sub>2</sub> Compounds Under Compressive Stress." Journal of Magnetism and Magnetic Materials 31-34, pp. 849-851, 1983.
24. Clark, A.E., "Magnetostrictive Rare Earth - Fe<sub>2</sub> Compounds." Ferromagnetic Materials, Vol. 1, North Holland Publishing Company, Ames, Iowa, 1980.
25. Edge Technologies Brochure, Ames, IA, 1987.